

Copyright
by

John E. Porterfield

2010

The Dissertation Committee for John E. Porterfield Certifies that this is the approved version of the following dissertation:

**ADMITTANCE MEASUREMENT FOR EARLY DETECTION OF CONGESTIVE
HEART FAILURE**

Committee:

John A. Pearce, Supervisor

Jonathan W. Valvano

Ali Yilmaz

H. Grady Rylander

Marc D. Feldman

**ADMITTANCE MEASUREMENT FOR EARLY DETECTION OF CONGESTIVE
HEART FAILURE**

by

John E. Porterfield, B.S.; M.S.E.

Dissertation

Presented to the Faculty of the Graduate School of

The University of Texas at Austin

in Partial Fulfillment

of the Requirements

for the Degree of

Doctor of Philosophy

The University of Texas at Austin

May, 2010

Acknowledgements

As my advisor Dr. John A. Pearce notes, one should never write the word “we” in a dissertation, unless planning on splitting the degree with colleagues. This is perhaps why there is an acknowledgements section. As with many scientists, I feel like I have seen further because I have stood on the shoulders of the following giants:

Dr. Pearce is the person most directly responsible for making me a meticulous experimentalist. It is through his guidance that I have learned to do good science. I hope that someday I will be known for the kind of calculated intelligence he is known for.

Dr. Jonathan W. Valvano funded nearly my entire graduate career with Teaching Assistant funding. He is the reason I decided to come to Texas, and continues to give great advice and support in more areas than just academics. There is a good reason why his class continues to be one of the most popular in our department. He is also one of the kindest professors I have ever met and I hope that someday I’ll be as good of a mentor to someone as he was to me.

Dr. Marc D. Feldman is the most called number on my cell phone, and has been for years. I have learned more about cardiology from him than I could have ever learned from a class, and he is the reason my publications can cross disciplines like medicine and engineering seamlessly. I don’t know if it will ever happen, but I hope that someday I’ll be known for having the type of passion he has for his work.

I'm quite convinced after learning about experiences at other schools that I am incredibly lucky to have had not one, but three advisers who care deeply about my work.

My colleagues have been an important source of inspiration and I may have learned as much from them as my professors. From Anil T.G. Kottam I learned how to perform the perfect experiment. His tenacity and insight is unmatched in the laboratory. From Karthik Raghavan I learned the limits of overwork (which I have not come close to hitting), and how to be happy against all odds. He is a learned man. From Erik R. Larson I learned humility in the face of error. I have probably been proven wrong many more times than I care to admit by him, and I am a better scientist, and a better person because of it.

I have worked with over 12 surgeons throughout my graduate career, and I was lucky enough to have the best 2 working on my experiments, Danny Escobedo and Sander Hacker. Their support staff at the LAR in San Antonio is my idea of the perfect team, including Travis Jenkins, Rudy Trevino, and Kelsey Johnson.

Last but not least, I'd like to thank my family for standing by me through good times and bad. I know that I come from a long line of careful thinkers, and my success is because of the things they've taught me. My mother, Salome Porterfield, taught me to read, sent me to good schools, and formed my strength of character. I was always inspired by the fact that she is and was a working mom. My father, Jim Porterfield, taught me every important lesson I need to make tough decisions every day. His advice is still worth the most to me. My brothers James and Jason Porterfield keep me grounded and sane. Even without schooling I would have turned out a good person because I am blessed to have such a great family.

Admittance Measurement for Early Detection of Congestive Heart Failure

Publication No. _____

John E. Porterfield, Ph.D.

The University of Texas at Austin, 2010

Supervisor: John A. Pearce

Impedance has been used as a tool for cardiac research since the early 1940's. Recently there have been many advances in this field in the diagnosis of human heart failure through the measurement of pacemaker and ICD coupled impedance detection to determine the state of pulmonary edema in patients through drops in lung impedance. These new detection methods are far downstream of the initial changes in physiology, which signify heart failure risk, namely, an increased left ventricular (LV) end-diastolic volume (also known as preload). This dissertation presents the first formal validation of the complex admittance technique for more accurate blood volume measurement *in vivo* in mice. It aims to determine a new configuration of admittance measurement in a large scale animal model (pigs). It also aims to prove that "piggybacking" an admittance measurement system onto previously implanted AICD and bi-ventricular pacemakers is a feasible and practical measurement that will serve as an early warning system for impending heart failure through the measurement of LV

preload, which appears before the currently measured drop in lung impedance using previous techniques.

Table of Contents

Table of Tables.....	x
Table of Figures	xi
Chapter 1: Admittance for Heart Failure Detection	1
1.1 Motivation	1
1.2 Background.....	2
1.3 Specific Aims.....	14
1.4 Chapter Overview.....	15
Chapter 2: Experimental Validation of Admittance and Wei’s Equation.....	16
2.1 Introduction.....	16
2.2 Methods	16
2.3 Results	23
2.4 Discussion	35
Chapter 3: Large Scale LV Catheter Volume Measurement and Modeling	42
3.1 Introduction.....	42
3.2 Methods	44
3.3 Finite Element Model (FEM) Definition	48
3.4 Boundary Conditions	48
3.5 Field Uniformity and its Effect on Volume Measurement.....	50
3.6 Modeling Conclusions.....	53
Chapter 4: Epicardial Preload Measurement Theory and Modeling	55
4.1 Introduction.....	55
4.2 Circuit Model	55
4.3 Impedance (Z) Separation of Blood and Muscle Components.....	57
4.4 Confounding Variables	59
4.5 Geometry of FEM Analysis.....	60

4.6	Sensitivity to Surgical Positioning Error	62
Chapter 5:	Epicardial Volume <i>in vivo</i> Experiments	64
5.1	Introduction –Animal Model of Congestive Heart Failure	64
5.2	Methods	65
5.3	Results	79
5.4	Discussion	85
Chapter 6:	Conclusion and Future Work	90
6.1	Future Work.....	90
6.2	Conclusion	91
Appendix 1:	Full Protocols	93
7.1	Open Chest Acute Preparation in Pigs	93
7.2	Closed Chest Acute Contractility Studies in Mice	94
7.3	Open Chest 1 wk Aortic Band Heart Failure Mice	96
References.....		98
Vita		104

Table of Tables

Table 1: Catheter position for each mouse	25
Table 2: Mesh Properties	47
Table 3: Electrical Properties	48
Table 4. LAD Occlusion.	83
Table 5. Ao Occlusion	84
Table 6. Pleural Effusion Simulation	85

Table of Figures

Figure 1: Tetrapolar catheter measurement of volume within the myocardium.	3
Figure 2: A typical cuvette calibration and matching Finite Element Model.....	7
Figure 3: A simplified diagram to explain how phase (θ) is measured is shown.	10
Figure 4: Tetrapolar surface probe.....	18
Figure 5: Representative mouse echo.....	19
Figure 6: Pressure-Volume loops from mice with catheter positioned off-center.....	27
Figure 7: Bland-Altman plot of echo vs. admittance volume.	29
Figure 8: Example preload reduction.	32
Figure 9: Representative example demonstrating that admittance is more sensitive.....	34
Figure 10: α plotted versus time.	37
Figure 11: A Multipolar catheter with segments chosen as in Baan's first study.....	42
Figure 12: FEM Model 2D axisymmetric geometry; distal section of the catheter.	45
Figure 13: 2D axisymmetric mesh	46
Figure 14: Closer view of one electrode, refined mesh.....	47
Figure 15 A: 1 mL cuvette and B: 100 mL cuvette current density (streamlines) and developed potential maps.....	50
Figure 16: Nonlinearity of the Conductance-Volume Relationship in large animals.....	52
Figure 17: The Alpha – Conductance graph is nonlinear in large animals.....	53
Figure 18: Epicardial circuit model	56
Figure 19: 3D model geometry of FEM.....	61
Figure 20: Potential Current Density streamline plot of FEM results.....	62
Figure 21: Results of Electrode positioning sensitivity experiment.....	63
Figure 22. Pacemaker electrode positioning.	66
Figure 23: Detailed experimental electrode positioning.	70
Figure 24. Typical Neosynephrine dose-response (Neo D-R) data	81

Figure 25. Neosynephrine dose-response for all datasets82

Chapter 1: Admittance for Heart Failure Detection

1.1 MOTIVATION

Heart disease is the leading cause of death in the United States [1]. Because of the current drive to treat the many forms of heart disease, life spans in patients have been extended and a shift is occurring from heart disease to heart failure in the affected population. At age 40, the lifetime risk of developing Congestive Heart Failure (CHF) is 1 in 5. As a result, a large portion of medical resources are currently used in the care and treatment of these patients.

Heart failure (HF) is the most common cause of admission to the hospital in the United States, and is the leading cause of death in the nation. In 2009, the American Heart Association estimates that more than \$37 billion was spent on HF in the U.S. alone in direct and indirect costs; and 1 in 8 deaths mention HF on the death certificate [2]. As the U.S. population ages and the number of persons surviving long-term with cardiovascular disease increases, the number of persons with heart failure is expected to grow dramatically, as are the number and cost of hospital admissions for heart failure.

Despite the established ability of pharmacotherapy to reduce hospitalizations, and the accepted importance of dietary sodium restriction and daily weight monitoring, the expected benefit of these therapies is not being realized. Episodic office-based management by physicians is often inadequate to provide needed long-term continuity of care, especially in older persons with multiple co-morbid conditions taking multiple prescribed drugs. Clinician under-prescribing and under-dosing of medications; patient non-adherence to drug regimens, self-monitoring of diet and weight, and lack of regular monitoring by healthcare providers contribute to many heart failure hospital

admissions. It is estimated that 50% of HF admissions may be avoidable. Since many of these patients will be receiving AICDs and bi-ventricular pacemakers, “piggybacking” a solution onto these devices will provide information regarding heart failure status that is needed to reduce both the number of hospitalizations, and the billions of dollars in cost for these hospitalizations.

1.2 BACKGROUND

Conductance measurements have been available as an invasive tool to detect instantaneous left and right ventricular volume since 1981 [3, 4] and a number of relevant publications have come from our group at The University of Texas at Austin [5-11]. Tetrapolar electrodes are typically placed on a catheter located within the heart chamber (i.e., the left ventricle, LV) to determine instantaneous volume. Conductance systems generate an electric field using a current source, and volume is estimated from the instantaneous voltage signal.

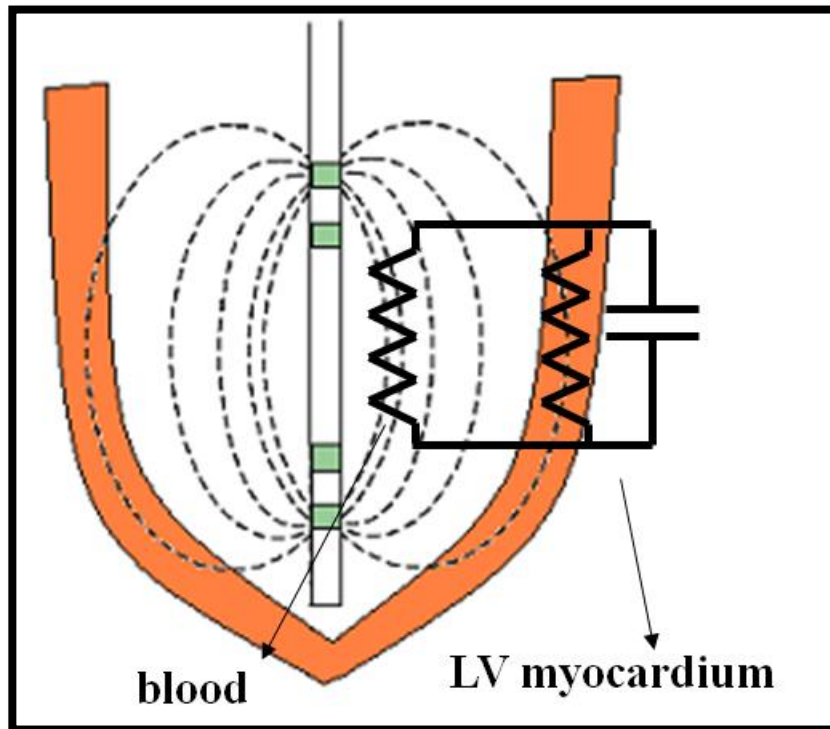


Figure 1: Tetrapolar catheter measurement of volume within the myocardium.

There is considerable debate in the scientific community about which equation to use for the conversion of conductance to volume, although most agree that the relationship between conductance and volume is nonlinear. Further, the conductance technique is limited as the conductance measured is a combination of both blood and surrounding myocardium, while only the blood conductance is desired to estimate volume. The myocardium is often called the “parallel conductance” because in the electrical model of an LV catheter measurement, the myocardium is essentially in parallel with the blood and the current source.

Making this measurement in humans *in vivo* is complicated because any catheter entry into the LV has an associated risk of causing emboli, which can lead to a stroke. However, there has previously been no way to interrogate the instantaneous volume of the LV using the conductance information without inserting a catheter. Conductance

electrodes have not been previously placed on the LV epicardium to interrogate the LV blood volume. This dissertation proposes the use of an admittance/impedance measurement system to separate the blood and muscle components from the combined voltage signal to estimate LV preload from previously implanted AICD and bi-ventricular pacemakers, for the first time.

1.2.1 Conductance to Volume Conversion Equations

The basis of volume estimation from conductance measurement is rooted in Electromagnetic Field Theory and can be explained with a simplified derivation. Start with the basic definition of equivalence resistance in a uniform electric field:

$$R = \frac{\rho L}{A} \quad (1)$$

The LV chamber will change in cross-sectional dimension as the heart beats ($A(t)$) which will provide a time-varying resistance signal ($R(t)$).

$$R(t) = \frac{\rho L}{A(t)} \quad (2)$$

The changing volume of the heart can be estimated from the field strength sensed at the voltage contacts. This is described as the cross-sectional area of the LV chamber multiplied by the length between the voltage contacts (a constant, in the case of a catheter measurement).

$$Vol = A(t) \times L \quad (3)$$

At this point one can rearrange equations (2) and (3) to produce Equation (4) below [12].

$$Vol = \frac{\rho L^2}{\alpha} (G - G_P) \quad \text{(Baan's Equation)} \quad (4)$$

The extra term α is a geometric correction factor for the assumptions made about the linearity of the field lines that justify the use of Equation (1), and is generally assumed to be dependent on the field shape. The \mathbf{E} field direction with respect to the LV major axis is along the myocardial wall, making the muscle a “parallel” conductance G_p . In most cases G_p is considered to be limited to the surrounding myocardium, because the conductivity of myocardium is much lower than that of blood, and because care is taken to make sure that the electrode spacing is small enough to constrain the field to essentially within the heart, but mostly in the blood pool. For example, longer current electrode spacing creates a larger sensing field and these longer spacings are used for larger hearts.

There are two major criticisms of Baan’s formulation. The first is that α , the calibration factor in Baan’s equation, is not a constant but instead changes dynamically as the moving heart wall changes the shape of the applied electric field [13]. The second is that as the LV contracts and fills, the cardiac muscle moves closer to and farther away from the catheter, so subtracting a constant G_p , as in Equation (4), probably does not adequately compensate for the parallel muscle conductance [13]. The latter problem is exacerbated by the aortic valve being off center relative to the midline of the LV chamber in mammalian hearts. This forces the miniaturized PV catheter to be closer to the septum than the midline [14]. Additionally, preload reduction used to generate load-independent measures of contractility is anticipated to further exacerbate any error from the currently practiced constant measure of parallel conductance. All volume conversion techniques are based on Baan’s Equation (4), and are differentiated by how they treat the gain calibration (calculation of α) and offset calibration (calculation of G_p). These differences are discussed next.

1.2.1.1 α Calibration

Baan's formulation assumes the field to be completely uniform; therefore the term α is set to 1 [3, 15]. This is referred to in the text as "no calibration." Baan argues that when looking at the end-systolic pressure volume relationship (ESPVR) to calculate measures of contractility, having an $\alpha = 1$ is adequate as long as inter-animal comparison is not necessary [4]. This may be true, but only because the slope of the ESPVR is not dependent on accurate absolute volume measurement, but rather on accurate volume difference measurement.

The simplest form of calibration is known as cuvette calibration, and is a direct 1 to 1 mapping from conductance to volume. The calibration is performed by measuring the conductance of blood in non-conductive cuvettes of known volume. The volumes should span the range of volume being measured *in vivo*. Because the volumes are known, a plot is then constructed of volume vs. conductance, and the slope of the line of best fit through all the data points is used for the value α . This fit line is then used for subsequent conversion of conductance to volume. Figure 2 below shows a typical cuvette calibration, and accompanying Finite Element model work which confirms it [Yi Mao, unpublished observation].

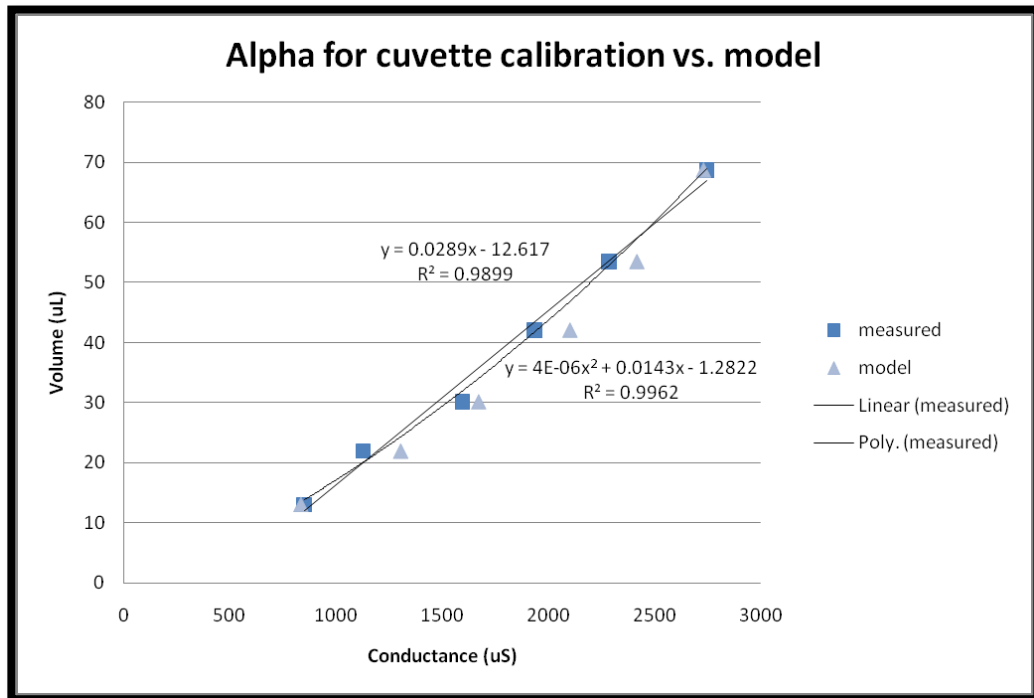


Figure 2: A typical cuvette calibration and matching Finite Element Model.

A more robust calibration of α is the stroke volume (SV) calibration. This method chooses a value of α that will force the SV of the converted volume signal to the true value of SV (derived from flow-probe measurements or echocardiography data) at baseline. Once the SV is known, α can then be calculated using Equation (5) below:

$$\alpha = \frac{\rho L^2 (G_{BED} - G_{BES})}{SV_{truth}} \quad (5)$$

where $G_{BED}-G_{BES}$ is the peak to peak change in conductance at baseline, and SV_{truth} is the measured true stroke volume at baseline. If the value of SV_{truth} changes during intervention, the values of G_{BED} and G_{BES} will also change, leaving α relatively unchanged.

There is a fourth type of calibration for α , which is also, in essence, a SV calibration; but also takes into account the relative values of G_{BED} and G_{BES} when calculating the final volume. It is “nonlinear” in the sense that the α term is no longer a constant, but is instead dependent on the blood conductance G_B . The equation can be re-written:

$$Vol = \frac{1}{1 - \frac{G_B}{\gamma}} \rho L^2 G_B \quad (6)$$

where γ is a new constant defined quadratically as:

$$\gamma = \frac{-b \pm \sqrt{b^2 - 4ac}}{2a} \quad (7)$$

where

$$\begin{aligned} a &= SV_{truth} - \rho L^2 (G_{BED} - G_{BES}) \\ b &= -SV_{truth} \times (G_{BED} + G_{BES}) \\ c &= SV_{truth} \times G_{BED} \times G_{BES}. \end{aligned} \quad (8)$$

Equations (6)-(8) are known collectively as Wei's equation, and have been previously published [16] and validated [17].

1.2.1.2 G_p calibration

Another major source of error in catheter measurements of blood volume is the effect of the myocardium and surrounding structures on the blood volume measurement, G_p . In Baan's equation this term is a calculated constant. The calculation of G_p is another distinguishing factor between the different methods of conductance to volume conversion.

Currently, the most popular way to calculate a constant G_p is through injection of a hypertonic saline (HS) bolus of high conductivity ($\sigma \approx 1-1.6$ S/m). The bolus of HS transiently changes the conductivity of blood *in vivo* as it passes through the circulatory system, and eventually into the LV. The blood conductance minima (G_{BES}) are then plotted against the maxima (G_{BED}) and back-projected to determine the point where $G_{BED} = G_{BES}$. This point is the value of G_p ; the point where the blood volume is zero, and conductance is unchanging. The method is outlined in more detail in previous studies [5].

Contrary to the assumptions of the HS method above, it has recently been proven that the parallel conductance from the myocardium does vary during the cardiac cycle [13], and this finding has been verified by other authors as well [5, 6, 11, 13]. This leads to error in the calculation of volume during the transition between V_{ED} and V_{ES} , and even greater errors during loading changes on the heart that might increase or decrease volumes at systole and diastole. To date, there is only one method that does take into account the dynamic nature of G_p , and this is the admittance method.

The admittance method makes use of the native capacitive properties unique to myocardium to identify its contribution to the measured signal so that it can be removed in real time without the need for hypertonic saline injection. The basis of measuring admittance (magnitude and phase) rather than conductance (magnitude

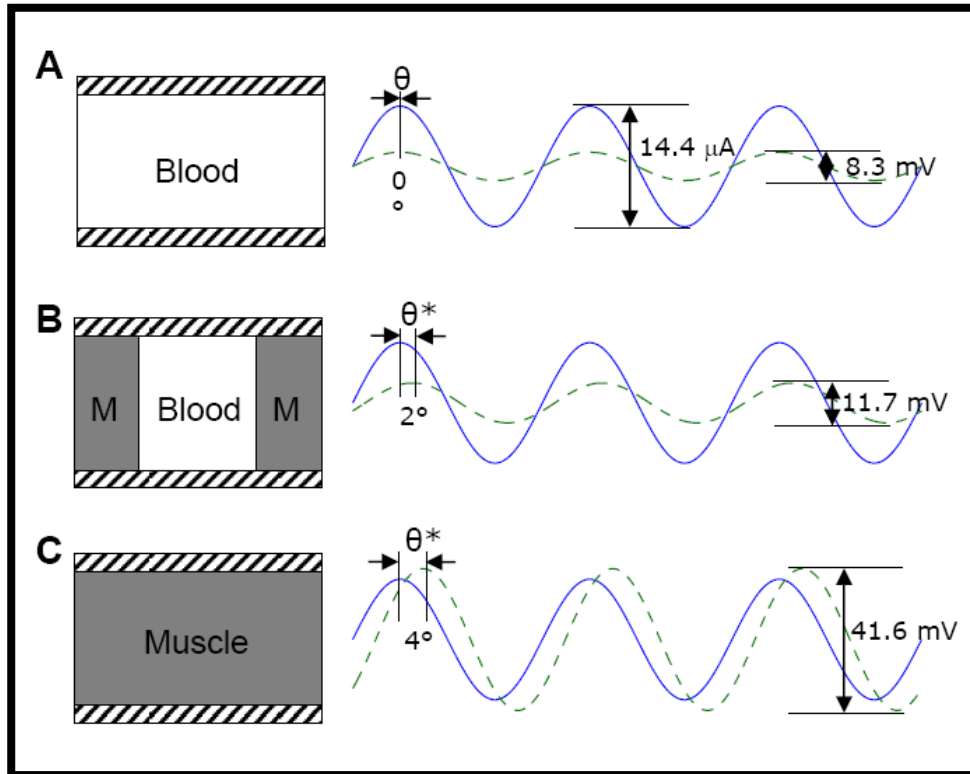


Figure 3: A simplified diagram to explain how phase (θ) is measured is shown. The conductance electrodes are demonstrated as planar metal electrodes surrounding homogenous media of either blood, myocardium, or both. The solid line is input current (μA), and the dotted line is output voltage (mV): **A.** Measurement of blood only, provides no phase shift (θ). **B.** Combination of blood and muscle has some phase θ , and a somewhat larger amplitude output voltage (implying lower total admittance magnitude, $Y = I/V$). **C.** Pure muscle results in the largest phase shift θ and largest amplitude output voltage (low admittance magnitude). Phase measurement allows the separation of blood and muscle (**B**) in real time.

only) is that at frequencies around $f = 20 \text{ kHz}$, it has been shown that blood is purely resistive and has no measurable capacitance, but myocardium has both capacitive and resistive properties (Figure 3, above) [7, 10, 13]. This observation allows separation of

the admittance of the myocardium from the combined admittance signal, using electric field theory.

For a vector electric field, \mathbf{E} , in homogeneous tissue, the conductance and capacitance between the electrodes that establish the field are given by:

$$G = \frac{I}{V} = \frac{\sigma \int_S \mathbf{E} \cdot d\mathbf{s}}{-\int_{P_2}^{P_1} \mathbf{E} \cdot d\mathbf{l}} = \sigma k \quad (9)$$

$$C = \frac{Q}{V} = \frac{\epsilon \int_S \mathbf{E} \cdot d\mathbf{s}}{-\int_{P_2}^{P_1} \mathbf{E} \cdot d\mathbf{l}} = \epsilon k \quad (10)$$

where: G = conductance (S), I = current (A), V = potential (V), σ = electrical conductivity (S/m), k = the field geometry factor (1/m), C = capacitance (F), and Q = charge (C). The integration is from one electrode to the other along a vector pathway, L , and the surface, S , encloses all of the current from the source electrode. For a homogeneous medium the measured conductance and capacitance are related by a simple ratio:

$$G = \frac{\sigma}{\epsilon} C. \quad (11)$$

Equation (11) is the central principle of the admittance method. The important ratio of σ/ϵ is determined by a surface probe measurement of the properties of myocardium, which is described in detail by Raghavan *et al.* [7].

Briefly, the imaginary part of the admittance is defined as

$$Im\{\vec{Y}\} = |\vec{Y}| \sin(\theta) = \omega C_{myocardium} + \omega C_{catheter} \quad (12)$$

Therefore, once the (purely imaginary) catheter contribution has been determined and subtracted through calibration in saline,

$$C_{myocardium} = \frac{|\vec{Y}| \sin(\theta)}{\omega}. \quad (13)$$

The real part of the admittance is

$$Re\{\vec{Y}\} = |\vec{Y}| \cos(\theta) = G_{blood} + G_{myocardium}. \quad (14)$$

Consequently,

$$G_{blood} = |\vec{Y}| \cos(\theta) - G_{myocardium} \quad (15)$$

where

$$G_{myocardium} = \frac{\sigma}{\epsilon} C_{myocardium} \quad (16)$$

Based on these equations, one can determine the instantaneous values of parallel conductance G_p , and therefore blood conductance (G_B). An example of how this is accomplished in experiment is detailed in Section 2.2.2.

1.2.2 Heart Failure Pathology

The *backward heart failure concept* was first proposed in 1832, and contends that when the LV fails to discharge its contents, blood accumulates and pressures rise in the atrium and venous system emptying into it [18]. The inability of the LV to shorten against a load alters the relationship between end-systolic pressure and volume so that LV end-systolic volume rises. The following sequence then occurs, which at first maintains cardiac output, but ultimately leads to clinical deterioration – (a) LV end diastolic volume and pressure increase, (b) the volume and pressure rise in the left atrium, (c) the left atrium contracts more vigorously (Starling’s Law), (d) the pressure in the pulmonary veins and capillary beds behind the LV rise, (e) transudation of fluid from the pulmonary capillary beds into the pulmonary interstitial space increases, (f) the elevation of LV, left atrial, and pulmonary venous pressures results in backward

transmission of pressures into the pulmonary arterial circuit and leads to pulmonary hypertension, and finally, (g) right heart failure then occurs as a consequence of left heart failure.

Further, as the LV fails, it will remodel to accommodate the increased load, to reduce chamber pressures. Preload is an important determinant of the progression of heart failure. It is defined as “the stretch of the individual sarcomere” [18]. This stretch is most practically estimated via the end-diastolic ventricular volume, diameter, and end-diastolic pressure. For example, an increased end-diastolic ventricular volume or diameter, or a higher end-diastolic pressure, would imply a larger preload. Increased LV preload is more easily detected than pressure elevation since the diastolic pressure-volume relation is relatively flat and produces a larger change in volume for a given change in pressure. This relationship is more evident as the LV remodels and dilates since the diastolic ventricular pressure-volume relation flattens in heart failure [19]. An increase in preload will also precede an elevation in right heart systolic pressures, due to the length-tension relationship of cardiac muscle, i.e., – muscle is stretched before generating greater systolic pressures [20]. Based on these arguments, it can be assumed that an increasing LV preload (increasing LV end-diastolic Volume, or LVEDV) will be the most sensitive measure, and earliest indicator of impending CHF.

1.2.3 Clinical Significance

Heart failure is a problem that greatly affects populations having implanted devices such as ICDs and pacemakers. Periodic LVEDV detection provides a way to detect impending heart failure before the disease debilitates the patient by progressing to other parts of the body. It is orders of magnitude cheaper in total cost than any other alternative of volume measurement when the pre-existing need for an implanted device

is considered. The major cost for LV volume detection using admittance will be the one time cost of the pacemaker/AICD itself, and will provide real time information that can be used for telemedicine. This decreases costs substantially both directly for the treating hospital, physician, and patient, but also indirectly, in resources such as hospital beds, and personnel for treatment [21]. In addition, the patient will receive treatment earlier, and quality of life will improve not only because of prevention of symptoms, but also because telemedicine will allow a reduction in the length of hospital stay.

1.2.4 Competing technologies

There are two proposed “piggybacked” heart failure warning systems placed on bi-ventricular pacemakers and AICDs to reduce hospital admissions. First, Chronicle[®] measures right heart pressures in an attempt to monitor increases that are indicative of heart failure [22-24]. Second, Optivol[®] uses lung impedance (conductance) measurements as an indication of pulmonary edema [25-28]. However, both are downstream measures of what will be an earlier indicator of impending heart failure – left ventricular (LV) preload or left ventricular end-diastolic volume (LVEDV). There are currently no proposed technologies that can perform chronic left ventricular volume measurements in part because implanted devices inside the left heart lead to arterial embolism and stroke.

1.3 SPECIFIC AIMS

The specific aims of this dissertation are: 1. To validate Admittance and Wei’s equation as the standard for catheterized heart volume measurement, both in small and large animal models. 2. To design through the use of computational modeling and experimentation, new configurations of admittance measurement that will mimic the standard pacemaker configuration, and 3. To investigate through experiment the

efficacy of an epicardial lead configuration for the detection of increased LV end-diastolic volume.

1.4 CHAPTER OVERVIEW

The traditional problems of the dynamic nature of G_p and α are addressed with the advent of Wei's equation, whose validation is the focus of the Chapter 2 of this dissertation. Chapter 3 deals with the extension of these principles to a larger scale animal model to prove its viability as a measurement in human-sized hearts, and also discusses the potential advantages and drawbacks of using more than four electrodes. Chapter 4 deals with the theory of how to make the admittance measurement in the new epicardial catheter configuration along with a discussion of surgical positioning error, and Chapter 5 deals with the validation of this new measurement through experiment *in vivo* in pigs.

Chapter 2: Experimental Validation of Admittance and Wei's Equation

2.1 INTRODUCTION

To confidently perform an indirect volume measurement of any kind, it is necessary to provide results against a known volume standard, usually MRI or ultrasound echo. Previously, the measurement of admittance for volume determination was validated through comparison with the previous standard method for conductance catheter determination [5], referred to in this dissertation as the “traditional conductance technique”. But traditional conductance is a flawed method at both a practical, and a theoretical level for two major reasons: 1) The “gain term” $1/\alpha$ in Baan's equation is not a constant, but instead changes dynamically as the moving heart wall changes the shape of the applied electric field, and 2) As the LV contracts and fills, the cardiac muscle moves closer to and farther away from the catheter, so subtracting a constant G_p (as in Baan's equation) does not adequately compensate for the parallel muscle conductance. For these reasons, a study to validate the admittance technique against a known standard must be performed using a better standard for volume measurement.

2.2 METHODS

2.2.1 LV Catheter Calibration

LV catheter calibration is necessary to determine the relative contribution of the catheter to the impedance measurement. The catheter and instrument both produce an additional phase shift, because they introduce additional capacitance to the volume measurement. The key to separation of muscle and blood signals lies in the phase measurement, so a calibration is performed to determine the artifact phase

contribution. The calibration performed allows quantification of both the catheter – and instrument – related phase and their effects on admittance magnitude.

The admittance system is calibrated by measuring the admittance magnitude and phase angle of both the tetrapolar and epicardial catheters immersed in varying conductivity saline solutions (1000, 2000, 4000, 8000, 10000, and 12000 $\mu\text{S}/\text{cm}$). Saline is chosen for the calibration because it will not produce a measureable phase shift at this frequency, and because it is easy to produce solutions in the required range of conductivity. The range of conductivity of solutions is determined by including the smallest and largest values of conductivity expected in the *in vivo* mouse heart, which ranges from 1600 $\mu\text{S}/\text{cm}$ for myocardium to approximately 10000 $\mu\text{S}/\text{cm}$ for blood. The admittance measurement is a parallel combination of the two. Thus, the admittance system phase calibration is designed to cover this entire range. The containers for the saline solutions are much greater in diameter than the distance between the voltage electrodes, so that the electric field produced by the current is essentially unconstrained by the sides of the container. The values measured for admittance magnitude and phase are therefore independent of the shape of the saline container, and only dependent on the measurement hardware and the conductivity of the solution.

Additionally, the relationship between G and σ is determined from this calibration information via Equation (9). It is important to make sure that the value of the field form factor (k) is constant with changing conductivity, because k should be dependent only on the field geometry, which should not change as the conductivity

changes in a cuvette of large size.¹ Variability in k could indicate that there are strange interface effects at work, or that the catheter is damaged in some way.

2.2.2 Muscle Properties Measurement Calibration

Muscle properties are measured using a surface probe that rests on the surface of the myocardium and has a field that penetrates only the tissue and not into the underlying blood pool. The theory is outlined in Equations (11) through (14), with the exception that the real part of the admittance in this calibration only includes the conductance of the muscle.

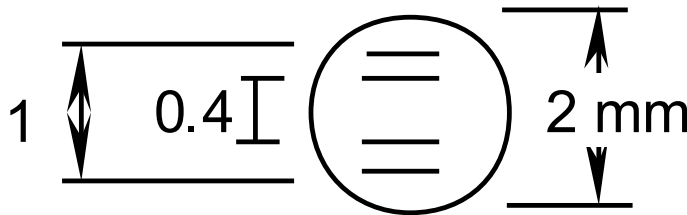


Figure 4: Tetrapolar surface probe used for epicardial admittance measurements, to determine the ϵ_m/σ_m ratio; mouse size.

The field does not penetrate into the blood below because the purposeful design of the surface probe current electrode spacing confines the field to the myocardium. The penetration depth is directly

dependent only on the conductivity of muscle and the electrode spacing. Using FEM simulation, a spacing is chosen for the surface probe electrodes that matches the thickness of the myocardium of interest, and the conductivity of muscle (normally around 0.15-0.2 S/m) [29]. The electrode effective depth of penetration is determined experimentally in saline over a non-conducting substrate, such as a glass microscope slide [30].

¹ Obviously this does not apply in a traditional cuvette calibration (a currently very popular technique), where calibration involves determining the change in conductance vs. field constriction in varying sizes of cuvettes.

2.2.3 Admittance vs. Hypertonic Saline Conductance vs. Cuvette vs. Echo Protocol

Mice were anesthetized by administration of 1-2% Isoflurane and were allowed to breathe spontaneously with 100% supplemental O₂. The right carotid artery was entered and a tetrapolar micro-manometer catheter (Scisense, Inc., London, Ontario) was advanced into the LV of the intact beating mouse heart. The right jugular vein was cannulated for later administration of 10 µl of 3% hypertonic saline to determine steady state parallel conductance. A total of n = 8 mice were studied. The position of the tetrapolar catheter in the LV was guided by simultaneous imaging with a transthoracic echocardiogram (VisualSonics, Toronto, Canada). The initial position for placement of the tetrapolar catheter was the off-center location (see Figure 5B).

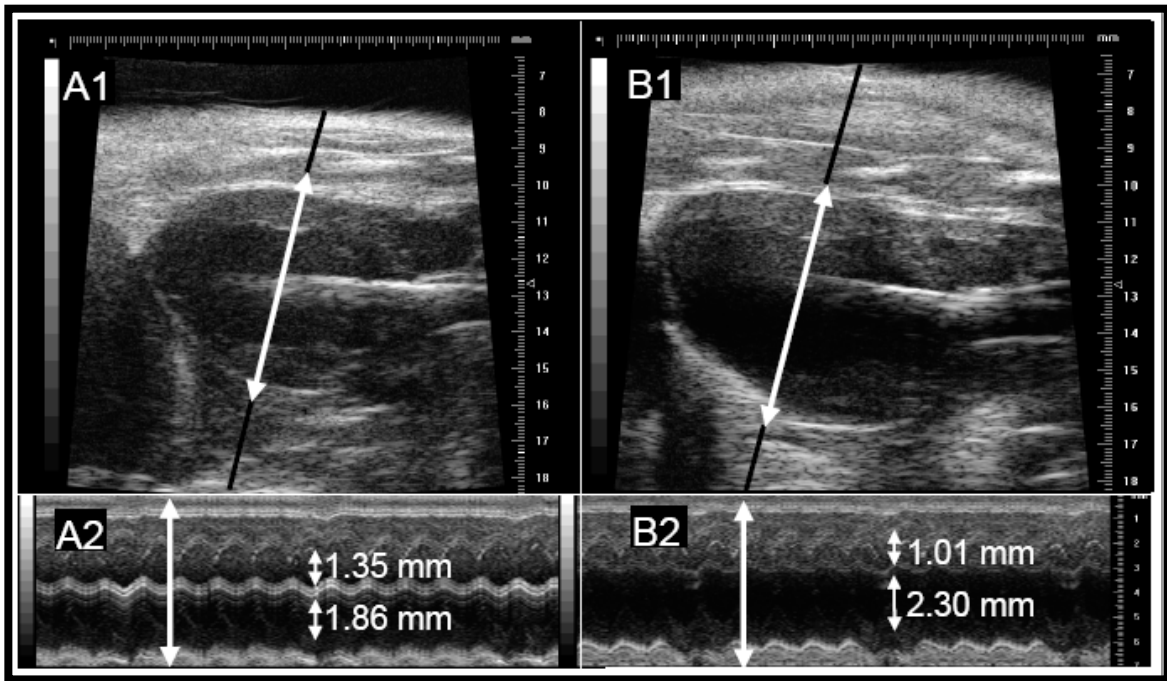


Figure 5: Representative mouse echo. A. Center positioned catheter guided by echo. **A1.** Long axis view **A2.** M-Mode view. **B.** Off-center positioned catheter guided by echo. **B1.** Long axis view **B2.** M-Mode view. M-Mode views quantify catheter to myocardium distances in mm. White double-headed arrows in long axis view indicate the line of M-Mode measurement.

In the off-center position, instantaneous LV PV relations were monitored to assure that a physiologic loop was obtained before acquiring data for both the admittance and conductance raw signals. Final acceptance of the catheter position was based upon both echocardiography and the appearance of the loop. Data acquisition consisted of simultaneous LV pressure, conductance (no phase) stimulated at 20 kHz, and complex admittance (magnitude and phase) also at 20 kHz, and echocardiographic images plus ECG for later calculation of end-diastolic volume (EDV), end-systolic volume (ESV), and stroke volume (SV). An operating frequency of 20 to 25 kHz maximizes the observable muscle signal [7]. All data were sampled at 1 kHz.

Subsequently, the tetrapolar catheter was re-positioned to be in the center of the left ventricular cavity (see Figure 5A), with final positioning confirmed by both echocardiography and a physiologic LV PV loop. Data acquisition for simultaneous LV pressure, conductance, admittance, and echocardiographic images plus ECG for later calculation of EDV, ESV, and SV were repeated. A 10 μ l bolus of 3% hypertonic saline was administered n=3 times per mouse via the right jugular vein, for later determination of steady state parallel conductance, as previously described [5]

2.2.4 Dobutamine Studies

A study was performed in n=6 mice (C57BlkS/J, female, body weight 23 ± 2.5 g, 8.7 ± 3 mos.) to determine the relative sensitivity of the admittance and conductance techniques to a contractility change induced by dobutamine infusion. Mice were anesthetized by administration of urethane (1000 mg/kg IP) and etomidate (25 mg/kg IP). Complex admittance (magnitude and phase) and conductance (magnitude only) with left ventricular pressure were obtained at steady state and during occlusion of the IVC at both baseline and during administration of $5\mu\text{g}/\text{kg}/\text{min}$ of dobutamine through the

jugular vein. Data acquisition for dobutamine was started 5 minutes after initiation of the IV infusion. Volume data were calibrated using flow probe-derived stroke volume at the end of each experiment, and subsequently converted to left ventricular volume using both Baan's equation, and Wei's equation. Parallel conductance G_p for Baan's equation was calculated as the constant mean value of the admittance-derived parallel conductance $G_p(t)$ to avoid blood conductivity changes due to the injection of hypertonic saline.

2.2.5 Aortic Banding and Heart Failure

In a separate experiment, $n=6$ mice underwent aortic banding for 1 week to increase the afterload (increase arterial resistance) on the LV, thereby changing the shape of the LV chamber over time. Muscle properties were examined as above, and volume was determined using the admittance method and compared to echo in this disease model.

2.2.6 Statistics

EDV and ESV derived by Wei's equation using admittance transient $G_p(t)$ were compared with echo data for EDV and ESV at both the centered and off-center positions using a two-sample right-tailed student's t-test. All calculations were performed using Matlab software (The Mathworks Inc., Natick MA). EDV and ESV derived by Baan's equation using hypertonic saline G_p were also compared with echo data using the same methods at both the centered and off-center positions. These analyses are also presented as Bland-Altman plots. Enhancement in contractility in response to dobutamine between baseline and drug infusion for both Baan's equation (SV calibration of α) and Wei's equation using admittance $G_p(t)$ were compared with

student's t-tests. The alteration in myocardial properties between control and aortic banded mice were also compared with student's t-tests.

2.2.7 Echocardiographic Calculations

2.2.7.1 EDV and ESV

End-diastole was defined as just after the peak of the R wave on the ECG, and end-systole was defined as minimum LV volume. A long axis view was taken for both end-systole and end-diastole, and the volume measured was determined using the cardiac analysis package from the Vevo 770 software (VisualSonics, Toronto, Canada). The long axis, and a single short axis within a long axis view were measured (see Figure 5A1 and B1), the second short axis was assumed to be of equal length. Volume was then computed using the prolate ellipse method [31, 32]. SV was determined as the difference between EDV and ESV, and was used in the calculation of both conductance and admittance derived LV volume.

2.2.7.2 Center and Off-center Catheter Positions

Both center and off-center positions were studied since placement of the miniaturized PV catheter across the aortic valve *in vivo* forces catheter placement near the septum and off the true LV center [14]. Thus, without echo guidance, the off-center position may be the position most often used by investigators.

To allow for comparison between a centered position and an off-center catheter position, the distance between the LV free-wall (LVFW) and the center of the catheter was measured, as was the distance between the center of the catheter and the septum (SEP). An example of these measurements is displayed in Figure 5A2 and B2. The percentage deviation from the center was calculated as:

$$Dev = abs\left(1 - 2 \times \left(\frac{LVFW}{LVFW + SEP}\right)\right) \times 100\% \quad (17)$$

In this calculation, a value of 100% indicates that the catheter position coincides with the inner myocardial wall, and a value of 0% indicates that the catheter is in the center of the ventricle. Catheter positions that are symmetric around the long axis result in the same percentage deviation from the center.

2.3 RESULTS

2.3.1 Myocardial Properties Measurement

The conductivity and permittivity of myocardium were measured in separate experiments in n=7 mice in an open chest preparation as described in [33]. The permittivity of myocardium derived from these measurements at 20 kHz was $\epsilon_m = (11800 \pm 2700) * \epsilon_0$ F/m, and the electrical conductivity of myocardium was measured at $\sigma_m = 0.160 \pm 0.046$ S/m. These results were used in calculations related to the admittance – conductance – echocardiography comparisons.

In an additional n=9 mice, the impact of left ventricular hypertrophy (aortic banding for 1 week) on myocardial properties was determined. Heart weight (86 ± 4 mg control, 124 ± 7 mg banded $p < 0.0001$) and LV weight (70 ± 7 mg control vs. 109 ± 10 mg banded $p < 0.001$) increased with banding. In n=4 banded mice, $\epsilon_m = (16726 \pm 9492) * \epsilon_0$ F/m, an increase of $(7450 \pm 6703) * \epsilon_0$ F/m from age and sex matched controls (n=5, $p < 0.05$). The myocardial conductivity showed no change from banded $\sigma_m = 0.184 \pm 0.042$ S/m to control $\sigma_m = 0.185 \pm 0.029$ S/m, $p = NS$.

2.3.2 Hemodynamic and Echocardiographic Parameters for Admittance – Conductance Comparison

For n=8 mice, the body weight ranged from 19 to 30 g (mean = 26.5 ± 3.5 g), heart weight ranged from 85 to 152 mg (mean = 123.8 ± 21.2 mg), and LV weight ranged from 67 to 107 mg (mean = 90.8 ± 14.6 mg). The mean left ventricular peak systolic pressure was 102 ± 10 mmHg, and the heart rate was 407 ± 28 bpm. The mean echo end-diastolic volume was 40.9 ± 12.1 μ l, and the mean echo end-systolic volume was 14.1 ± 5.5 μ l. The echocardiographic SV used in the calculation of both alpha (α) and gamma (γ) had a mean value of 26.8 ± 7.2 μ l.

The parallel conductance calculated by the hypertonic saline method was 476 ± 182 μ S, and by the admittance technique ranged dynamically from 552 ± 79 μ S at end-systole to 346 ± 67 μ S at end-diastole. The mean off-center α was 0.22 ± 0.15 as determined from echo SV, and it was 1.01 with cuvette (centered). The mean γ was 1350 ± 389 μ S. The location of the catheter position relative to the wall is shown in Table 1. The center technique was closer to the true mid-line than the off-center position ($p < 0.0001$) based on the M-mode echo measurements. Typical examples of echo center and off-center catheter positions are shown in Figure 5.

Mouse No.	Catheter Position*	
	Wall	Center
1	55%	20%
2	80%	21%
3	39%	16%
4	78%	3%
5	36%	0%
6	47%	23%
7	31%	18%
8	62%	9%
mean	53 ± 19%	14 ± 9%

Table 1: Catheter position for each mouse. *Percentages represent positional deviation from center. 0% = center, 100% = wall.

2.3.3 Wei's Equation Using Admittance is More Accurate than Baan's Equation Using HS and Either SV or Cuvette Calibration With Off-Center Catheter Placement

The off-center derived PV loops from Wei's equation, Baan's equation with SV calibration ($\alpha = 0.22 \pm 0.15$), and Baan's equation with cuvette calibration ($\alpha = 1$) for all $n=8$ mice are shown in Figure 6. As is visually apparent in 5 of these 8 mice, the SV calibrated conductance derived PV loops are to the right of echo (mice # 2, 4, 5, 7, 8), and the cuvette calibrated conductance loops are to the left of echo (mice # 1, 2, 3, 6, 7). In contrast, all of the Wei's equation with admittance loops are similar to the echo derived volumes. The end-diastolic and end-systolic volumes derived using Wei's equation ($\alpha(G_B) \approx 0.7-0.9$) show significantly less absolute error ($-2.49 \pm 15.33 \mu\text{l}$ error ES and ED) than the same quantities calculated using SV calibrated conductance ($\alpha \approx 0.1-0.3$) ($35.89 \pm 73.22 \mu\text{l}$ error ES and ED) or cuvette calibrated conductance ($\alpha = 1$) (-29.10

$\pm 31.53 \mu\text{l}$ error ED, and $-7.53 \pm 16.23 \mu\text{l}$ error ES), taking the echo volumes as the standard of comparison ($p < 0.03$).

These results are shown in graphical format as Bland-Altman plots in Figure 7A. The Bland-Altman plot shows that most of the error lies in the low repeatability (high standard deviation) of measurements when relying on Baan's equation with SV calibration. A consistently small absolute volume and stroke volume are observable in results from Baan's equation with cuvette calibration, which is consistent with observations in the literature [34, 35]. These results show that when the catheter is not placed in an optimal, i.e., central position, admittance provides an advantage in accuracy.

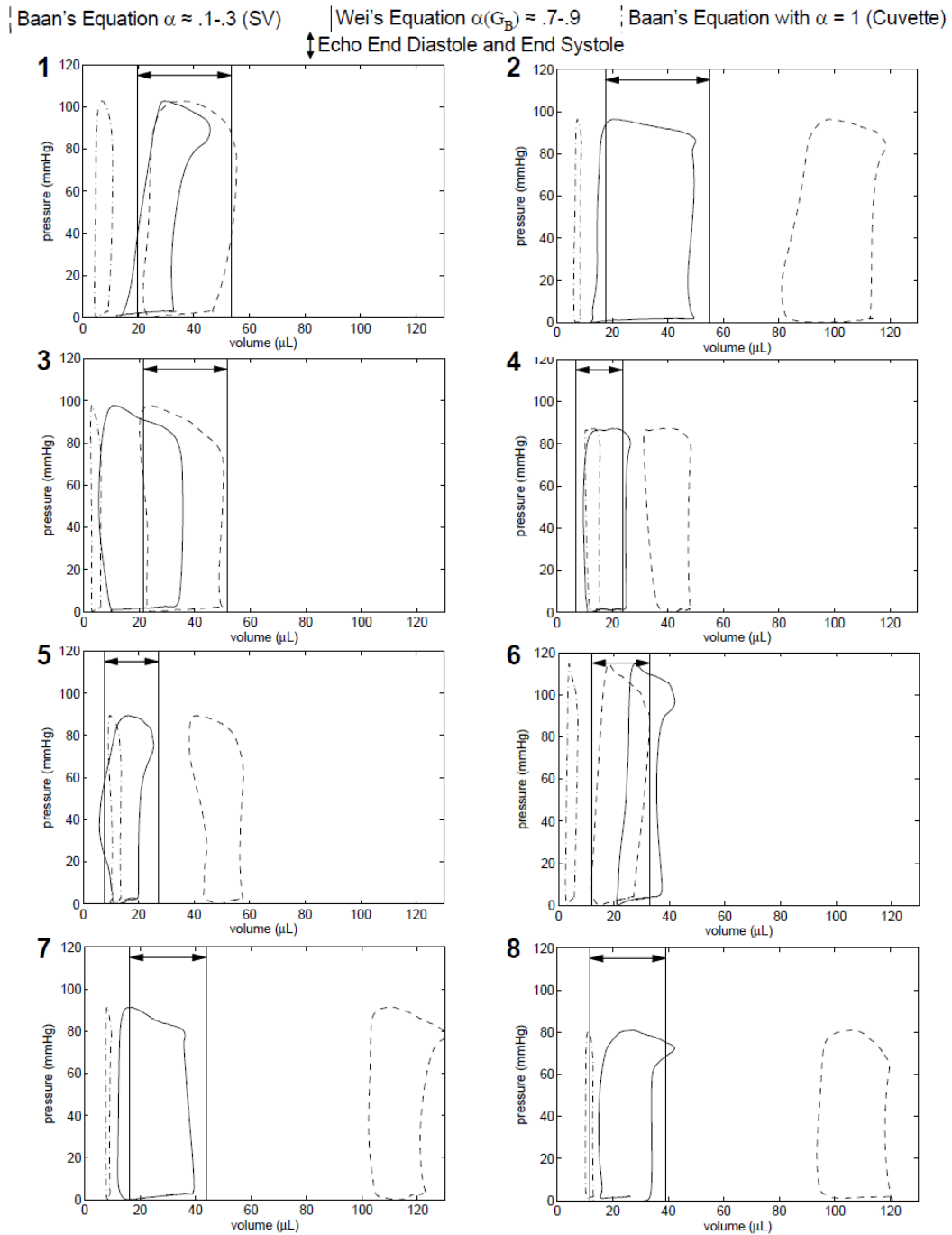


Figure 6: Pressure-Volume loops from mice with catheter positioned off-center. The solid lines represent the end-systolic and end-diastolic echo reference. The solid loops were derived with Wei's equation and admittance where $\alpha(G_B(t))$ is determined instantaneously, and ranges between 0.7 and 0.9 during the cardiac cycle; the dot-dash loops were derived using Baan's method of hypertonic saline with cuvette calibration ($\alpha = 1$); the dash loops were derived using Baan's method of hypertonic saline with echo SV calibration ($\alpha = 0.1 - 0.3$). As is visually evident, the admittance technique in combination with Wei's equation was closer to echo.

2.3.4 Wei's Equation Using Admittance is as Accurate as Baan's Equation Using HS and SV or Cuvette Calibration with Centered Catheter Placement

For the same 8 mice, when the catheter was shifted to the central position and the same measurements were taken, the same trend was observed: every Wei's equation/admittance PV loop gave a smaller volume than those derived from Baan's equation $\alpha = 0.22 \pm 0.15$ with HS, and larger than every PV loop from Baan's equation with $\alpha = 1$ using cuvette calibration (Figure 6). However, the difference in error between Wei's equation and echo measurement, and between both calibration methods for Baan's equation and echo, were not found to be statistically significant in either case with one exception: in the end diastolic measurements from cuvette calibration, Wei's equation shows lower error ($p < 0.03$). The closeness of these three results may be due to the removal of equivalent amounts of parallel conductance when the tetrapolar catheter is centered with echo guidance, where the average G_p using hypertonic saline is $476 \pm 182 \mu\text{S}$ vs. admittance's average $G_p(t)$ of $448 \pm 60 \mu\text{S}$. The mean of an instantaneously varying parallel conductance and an example real-time signal are shown in Figure 8A.

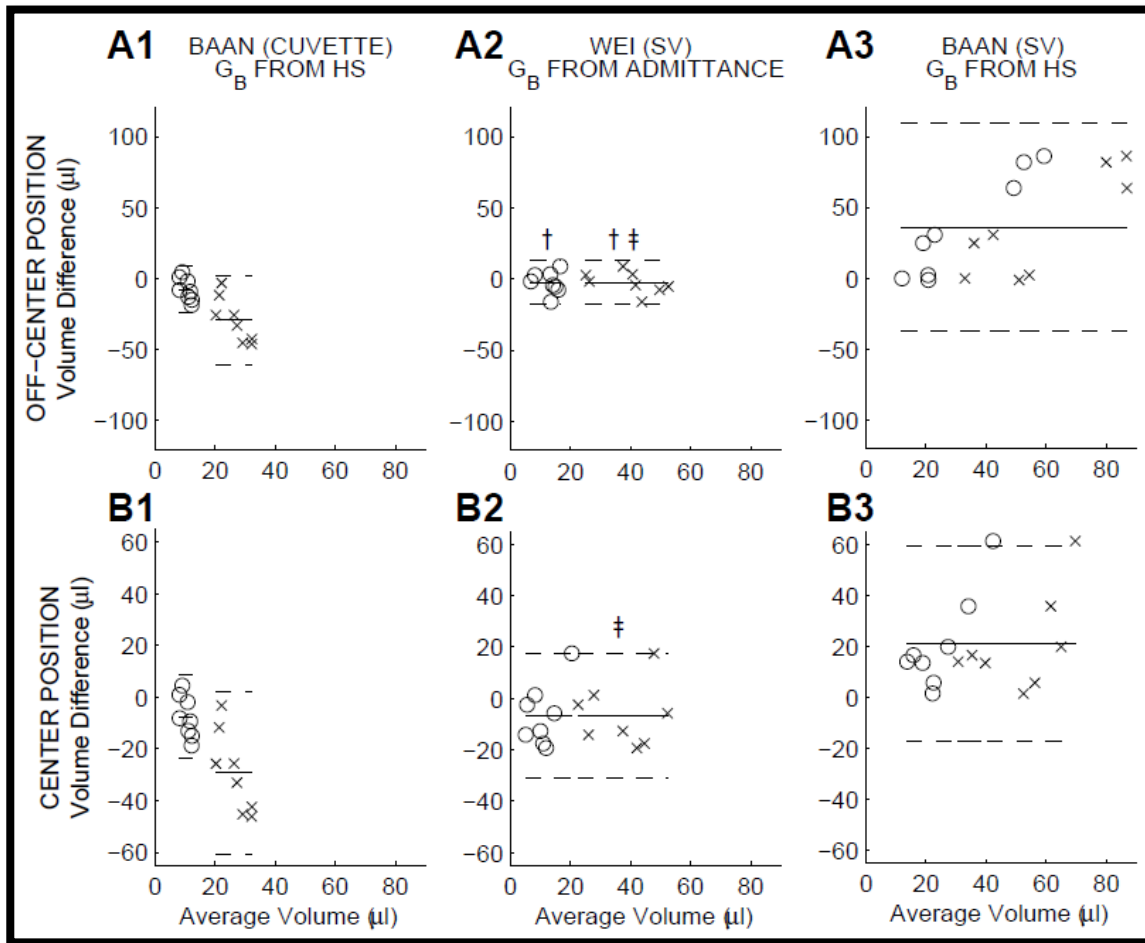


Figure 7: Bland-Altman plot of echo vs. admittance volume. The volume difference of each method vs. echo is plotted on the y-axis vs. the mean of echo and each method on the x-axis in these Bland Altman plots in n=8 mice for both End-Systolic (circle) and End-Diastolic (x) volume measured at A. the off-center position comparing A1. Volume from Baan's Equation using hypertonic saline vs. Echo volume (Average Error for ESV = $-7.54 \pm 16.23 \mu\text{l}$, and EDV = $-29 \pm 15.33 \mu\text{l}$), A2. Volume from Wei's Equation using admittance vs. echo volume, (Average Error for ESV and EDV are equivalent, Error = $-2.49 \pm 15.33 \mu\text{l}$), A3. Volume from Baan's Equation with echo SV calibration using hypertonic saline (Average Error for ESV and EDV are equivalent, Error = $35.89 \pm 73.22 \mu\text{l}$); and B. the same three plots with the catheter at the center position. B1. Average error for cuvette-calibrated conductance ESV = $-7.54 \pm 16.23 \mu\text{l}$, and EDV = $-29 \pm 15.33 \mu\text{l}$ B2. Average error for Admittance ESV and EDV are equivalent, Error = $-6.64 \pm 24.3 \mu\text{l}$. B3. Average error for SV-calibrated conductance ESV and EDV are equivalent, Error = $-20.96 \pm 38.42 \mu\text{l}$.

Solid lines represent means and dashed lines represent the 95% confidence intervals. †Less error than SV-calibrated conductance ($p < 0.03$ in a student's t-test). ‡Less error than cuvette-calibrated conductance ($p < 0.03$)

2.3.5 IVC Occlusions Show Dynamic Removal of a Non-Constant Parallel Conductance

In additional mice (n=4) IVC occlusions were performed to demonstrate the ability of the admittance technique to dynamically separate blood conductance and myocardium conductance. Figure 8A shows the typical separation of the blood and myocardial components during IVC occlusion in a single mouse using conductance and admittance techniques, and all four mice showed the same phenomenon. The observation from this figure, which represents a departure from traditional conductance theory, is that during an IVC occlusion the amount of myocardium in the sensing field increases while the blood component of conductance still decreases and dominates the total conductance signal. Traditional conductance methods assume a constant value for parallel conductance, which is demonstrated to be an inaccurate assumption by these data.

Preload reduction is commonly utilized to generate measures of left ventricular function such as the end-systolic elastance (E_{es}), diastolic chamber compliance, and others. It is hypothesized that calculated values of E_{es} and other parameters would be affected by the change from traditional conductance with Baan's equation, to admittance with Wei's equation. Thus, the impact of these two techniques on calculated hemodynamic parameters was analyzed for an identical transient occlusion of the inferior vena cava from a single mouse. Results are shown in Figure 8B. Despite the similarity in conductances in Figure 8C, the appearance of the loops in Figure 8B is significantly different.

Additionally, there was an increase in measures of contractility using the admittance technique. E_{es} rose from 3.4 to 15.4 mmHg/ μ l; maximum elastance rose from 12 to 25 mmHg/ μ l, and preload recruitable stroke work rose from 52 to 95

mmHg· μ l, conductance to admittance, respectively. Further, there was an increase in chamber stiffness from 0.061 sec⁻¹ with conductance to 0.076 sec⁻¹ by admittance.

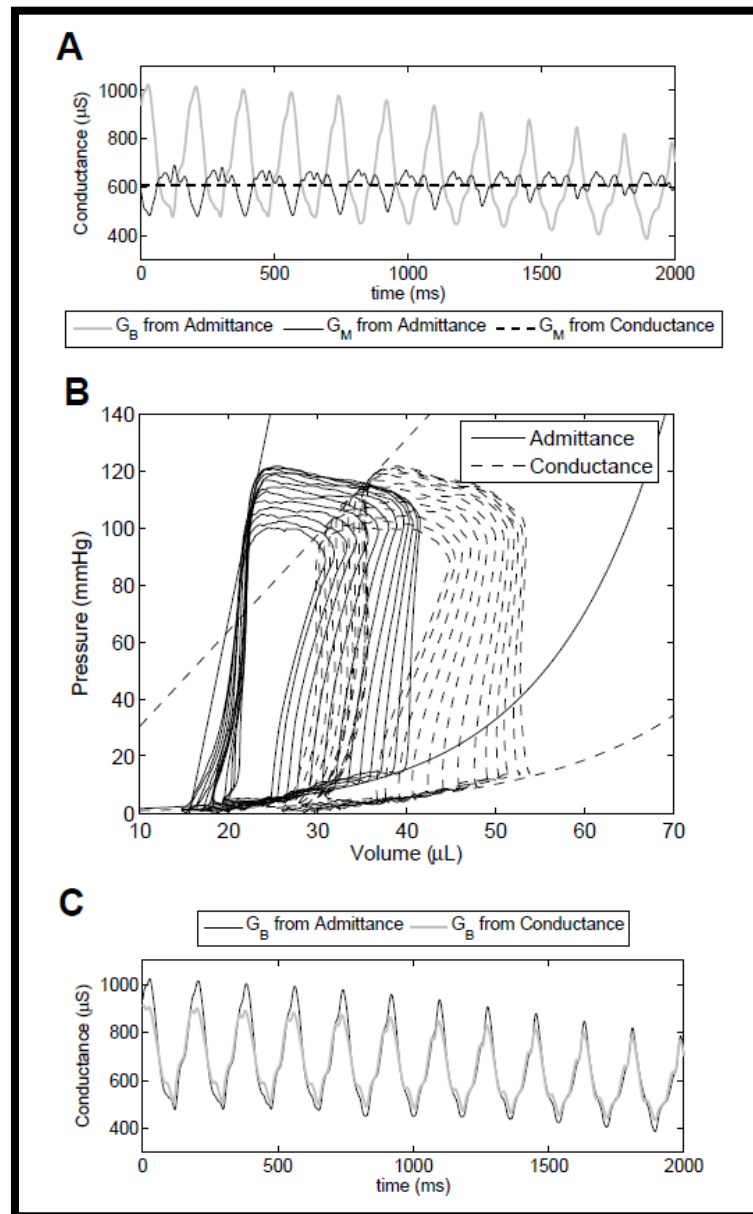


Figure 8: Example data from a single mouse during an identical preload reduction analyzed by constant G_p subtraction with Baan's equation (SV calibration of α), and admittance with Wei's equation are shown. A. The dynamic parallel conductance (G_M) computed by the admittance technique, is contrasted with the constant G_M subtracted by the conductance technique. The corrected conductance of blood (G_B) from admittance technique is also shown for reference. B. The data demonstrate differences in volumes and measures of contractility ESPVR for conductance $P_{ES} = 3.360 \cdot (V_{ES} - 0.942)$, and admittance $P_{ES} = 15.425 \cdot (V_{ES} - 15.566)$. Also shown are the EDPVR for conductance $P_{ED} = 4.797 \cdot 10^{-1} \cdot \exp(0.061 \cdot V_{ED})$ and admittance, $P_{ED} = 7.366 \cdot 10^{-1} \cdot \exp(0.076 \cdot V_{ED})$ C. The corrected conductance signals derived when admittance is used (a dynamic removal of parallel conductance), vs. conductance (a constant removal of parallel conductance).

2.3.6 Wei's Equation Using Admittance is more Sensitive to the Detection of Inotropic Stimulation

The hemodynamic response of n=6 mice was determined at baseline and following 5 minutes of steady infusion of 5 $\mu\text{g}/\text{kg}/\text{min}$ of iv dobutamine. Heart rate increased from 384 ± 47 to 523 ± 75 ($p < 0.05$). P_{max} was unchanged from 97 ± 13 to 98 ± 11 mm Hg ($p = \text{NS}$). dP/dt_{max} increased from $5,821 \pm 1,802$ to $12,309 \pm 3,832$ mm Hg sec^{-1} ($p < 0.01$), and dP/dt_{min} decreased from $-5,703 \pm 1,491$ to $-7,505 \pm 825$ mm Hg sec^{-1} ($p < 0.05$).

To evaluate the impact on parameters derived using Wei's equation and Baan's equation (both using SV calibration) during the identical IVCO, linear E_{es} and dP/dt -EDV were determined in these same mice. E_{es} is commonly used as a measure of the strength of the heart. E_{es} increased from 4.9 ± 1.4 to 12.5 ± 6.6 using Wei's equation ($p < 0.05$), and from 3.3 ± 1.2 to 8.8 ± 5.1 mmHg $\cdot \mu\text{l}^{-1}$ using Baan's equation ($p = \text{NS}$), implying that Wei's equation can pick up a strengthening of the heart while Baan's equation may not. A representative example is shown in Figure 9. Similarly, the dP/dt – EDV relationship increased from 158 ± 127 to 542 ± 320 using admittance ($p < 0.05$), and from 117 ± 78 to 263 ± 123 mmHg $\cdot \text{sec}^{-1} \cdot \mu\text{l}^{-1}$ using Baan's equation ($p = \text{NS}$).

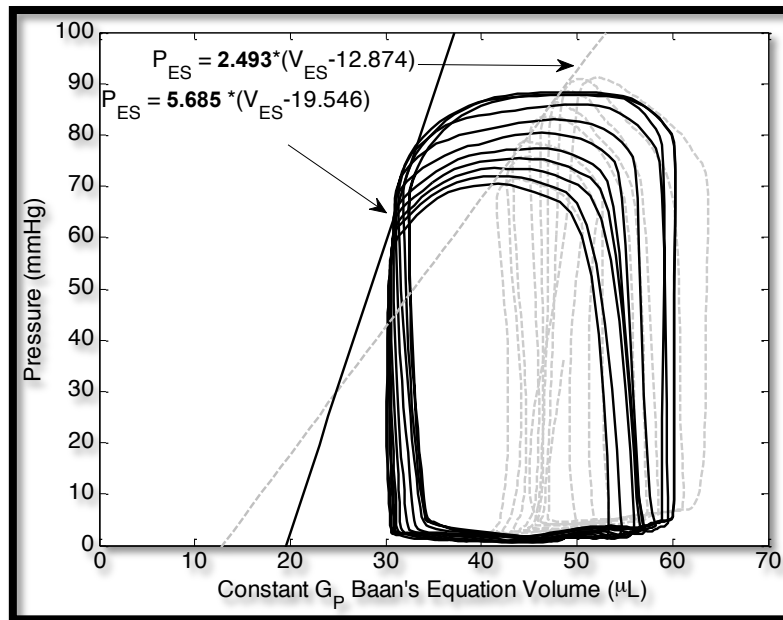
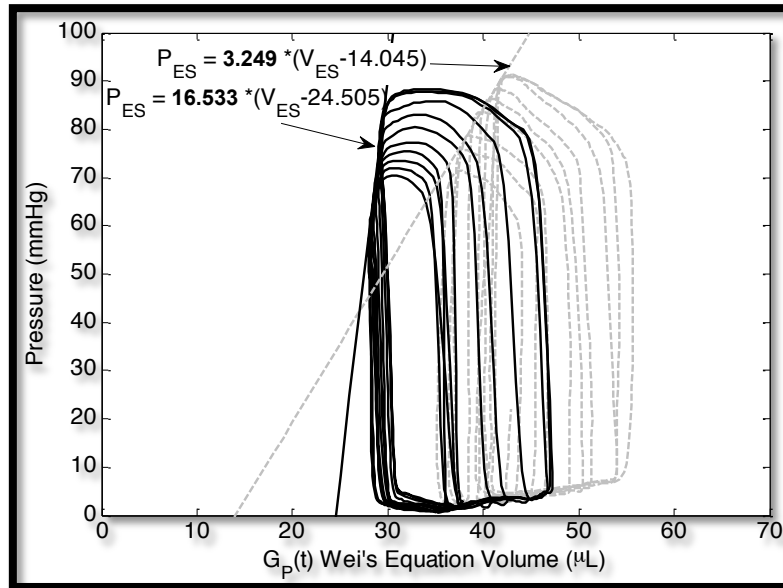


Figure 9: Representative example demonstrating that admittance (with Wei's equation, upper panel) is more sensitive in the detection of an increase in inotropy in response to iv dobutamine than Baan's equation (SV calibration of α , lower panel) during the identical IVCO in a single mouse. Similar results were found in n=6 mice (see text for discussion).

2.4 DISCUSSION

The results of this chapter compare the $V(t)$ determined by Baan's equation using G_p from HS with SV or cuvette calibration, to $V(t)$ determined by Wei's equation using admittance. In summary, it has been demonstrated that (1) more accurate volumes can be achieved with Wei's equation using admittance when the catheter is in the off-center position than Baan's equation using SV or cuvette calibration, (2) that the parallel conductance, G_p , varies between end-systole and end-diastole, and even more significantly during IVC occlusion, (3) the advantages of using a dynamically-changing α which is dependent on $G_B(t)$, and (4) improved sensitivity in the detection of inotropic stimulation with Wei's equation and $G_p(t)$ calculated using admittance, compared to Baan's equation and G_p calculated using HS with SV calibration of α .

2.4.1 Dynamic Parallel Conductance Calculation

In an early study by Lankford *et al.*, parallel conductance was demonstrated to be constant between end-diastole and end-systole [36]. Historically, this study was the theoretical basis for the acceptance of hypertonic saline injection determination of G_p in the literature. However, myocardium has both a conductive and a dynamic capacitive component [10, 11]. This concept is not reflected in the assumptions or conclusion of Lankford's study, nor in any traditional conductance technique where phase is not measured [4, 12, 14, 35, 37-39]. Mathematically speaking, the G_p calculated using admittance is a closer approximation to the true value of G_p than traditional conductance, because it takes into account the complex nature of myocardium $Y_p = G_p + j\omega C_p$, and therefore includes measurable changes during the cardiac cycle. The current results (Figure 8A) and Wei's previous study [11] imply that parallel conductance is

changing even between end-diastole and end-systole, as predicted by electric field theory [40].

2.4.2 Calculation of the Gain Term α

In the early conductance literature, the value of α was not calculated. α was assumed to be equal to 1, as described by Baan *et al* [4] and more recently by Uemura *et al* [41]. The purpose of the term α is to calibrate the stroke volume of the resulting conductance signal to match a standard of comparison (usually a flow probe, or echo). However, because α is dependent on the field geometry, and field geometry is constantly changing throughout the cardiac cycle, α is not a constant. As shown in Figure 10 during an IVC occlusion in a single mouse, the value of α differs depending on which calibration method is used.

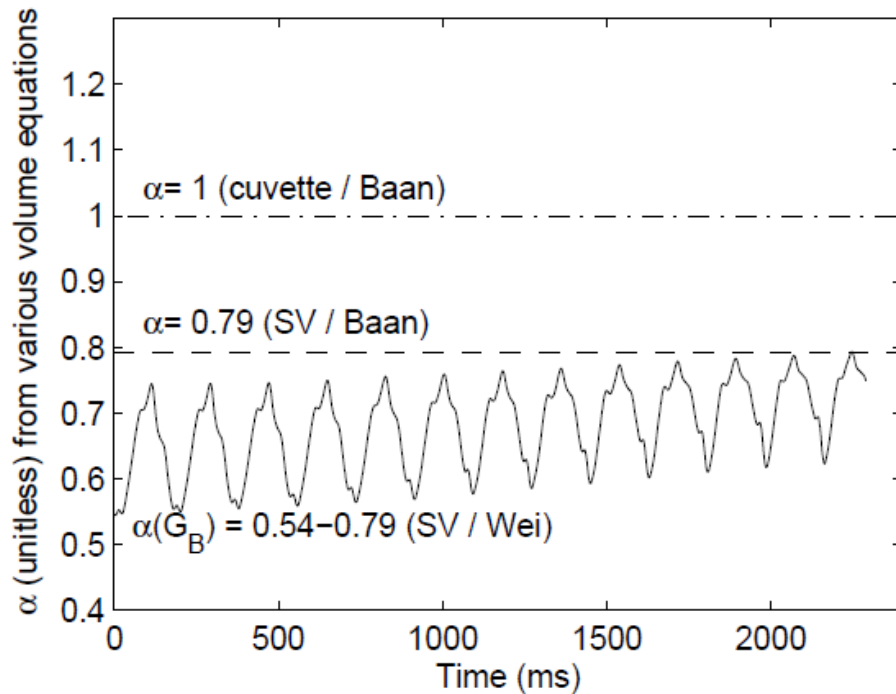


Figure 10: α plotted versus time from each of the three calibration methods during the same IVC occlusion as Figure 9. The dynamic nature of Wei's α is demonstrated to be in contrast with constant α as derived with either the cuvette or SV calibrated conductance techniques (using a flow probe to determine SV to calculate α).

For example, using Wei's equation, the dynamic nature of α is evident between systole and diastole, and also down the IVC occlusion ramp. In contrast, both other calibration procedures using flow or echo calibration ($\alpha = 0.79$ for centered position) and the volume cuvette method ($\alpha = 1$) – as recommended by manufacturers of the currently used commercial mouse conductance systems – use a constant value for α . The impact of using a variable α is that the volume equation will more closely model the changes which the field sees, as opposed to assuming a constant shape of the electric field.

2.4.3 Limitations of Cuvette Calibration

Review of the literature (122 publications) revealed that 63% of murine conductance studies utilize the volume cuvette as the calibration method of choice to

directly convert voltage to absolute volume [42]. However, recent studies [34, 35] have shown that cuvette-calibrated left-ventricular volumes are consistently smaller than those derived with a standard such as MRI, confirmed as well in the current study. Volume cuvettes have an electrically insulating boundary at the myocardial wall, which cramps the field causing an artificially high value of α (implying a small stroke volume). This high value of α causes small resultant volume estimates, and small resultant stroke volumes (See Figure 6).

2.4.4 Limitations of a constant α

A correction for the SV error introduced by the volume cuvette is to force the final SV to be the same as an independent measure. However, forcing only the SV to the independently verified value in an off-center position will reduce the value of α , increasing the “gain factor” (α^{-1}) of the volume equation. The benefit to the conductance technique is an accurate SV, but the detriment is an inflation of all volumes. As shown in Figure 6, although all SV are more physiologic when $\alpha = 0.22 \pm 0.15$, in mouse #2, 7, and 8, there is an inflation of volumes to an unphysiologic value. Although Figure 6 was generated from the off-center position of the miniaturized PV catheter, this is often the location of a catheter in the heart without echo guidance, since the aortic valve is off-center relative to the middle of the LV chamber.

2.4.5 Dynamically Changing α (Wei’s Equation)

The advantage of using a dynamic value for α is that more realistic volumes are obtained. As shown in Figure 6, incorporating a dynamic value for α provided absolute volumes closest to the echo standard. Wei’s equation provides a nonlinear conductance to volume relationship which has been noted in some recent papers [35]. However, the most significant improvement is that Wei’s $\alpha(G_B)$ is a function of blood conductance G_B

(see Equation 6) and γ . The derived value, γ , represents the value of conductance at saturation (where the catheter is placed in an arbitrarily large pool of conductive solution), so the expression $\alpha(G_B)$ incorporates the changing geometry of the electric field as the heart beats. This advantage of the γ -formulation will be particularly important when performing changes in loading conditions, such as IVC occlusion.

2.4.6 Wei's Equation Using Admittance $G_p(t)$ Improves Volume Estimates for Off-Center Placement of the PV Catheter

One assumption of Baan's equation is that the tetrapolar catheter is placed in the center of the left ventricle. However, the off center location of the aortic valve relative to the mid-LV chamber in mammalian hearts forces the miniaturized PV catheter to be closer to the septum [14]. Only the use of an independent imaging modality, such as echo, will allow a miniaturized PV catheter to be moved closer to the true center of the LV. Echocardiography, however, is not routinely used to center the conductance catheter. In the current study, despite the use of echo guidance, the mean central placement was actually $14 \pm 9\%$ at end-diastole, where 0% was true center and 100% is the LV free wall or septum. In addition, as the heart moves, one cannot assume that the catheter position stays at the midline. Some investigators estimate that the catheter shifts by 50-70% of the ventricular radius [43]. Thus, placement of the tetrapolar catheter in an off-center position is a common source of error.

In the present study, the off-center tetrapolar catheter Wei's equation using admittance $G_p(t)$ shows statistically less error than traditional conductance measurements taken simultaneously in a closed chest mouse, with simultaneous high frequency echocardiography used as the standard for true left ventricular volume. One explanation is that admittance provides a measure of instantaneous parallel conductance while all previous methods cannot. This is particularly evident in Figure 8A,

during occlusion of the inferior *vena cava*, where the myocardial component of the admittance signal is shown to vary both between end-diastole and end-systole, as well as during the occlusion ramp.

Additionally, the use of a dynamic value for α that is dependent on the value of conductance shows a more physiologic range for the absolute volume, while still matching the stroke volume of an independent method (usually flow probe or echo). In Baan's equation, the α term is dependent only on the conductance-derived SV. In Wei's equation however, the $\alpha(G_B)$ term is dependent on both the SV, and the current values of conductance. Figure 8B and Figure 8C demonstrate that this conclusion is only in part due to the differences in parallel conductance removal. In addition, the calculated volume ranges are quite different in Figure 8B, while the conductances shown in Figure 8C are similar, implying that the difference in the volumes is due to a difference in α as well.

As with any linear relationship, the slope α and the y-intercept G_p , are the only two points of control for the calibration of the volume signal using Baan's equation. This makes the accuracy of Baan's equation with hypertonic saline dependent on obtaining the correct values of α (which magnifies problems of using a constant α) and correct values of parallel conductance determined with hypertonic saline (which has a high relative error in the mouse) [4, 37].

2.4.7 Change in Myocardial Properties with Hypertrophy

The results of this chapter demonstrate that the permittivity (ϵ_m) increases by about 41% with LV hypertrophy induced by aortic banding for 1 week, while the myocardial conductivity (σ_m) did not change. The conductivity permittivity ratio (σ/ϵ), which is used in the central equation for admittance (the conductance capacitance

relationship), changes in these same mice from 69 S/ μ F in control to 17 S/ μ F in LV hypertrophy. It is known that larger myocytes have a greater membrane capacitance [44]. The measurement of capacitance in the electrode field increases during LV hypertrophy, thus a higher permittivity is inferred from the measurement. In the bulk tissue measurement, the increased permittivity detected is likely a summation of this increase in capacitance. Thus, it is critical to measure this σ/ϵ ratio in each group of mice with a different myocardial disease if the admittance technique is to derive LV volume accurately.

Chapter 3: Large Scale LV Catheter Volume Measurement and Modeling

3.1 INTRODUCTION

Large scale LV catheter volume measurement was invented well before the technique was miniaturized in mice, and the multi-electrode measurement of admittance is a natural extension of the tetrapolar technique in mice. To date, there have been no publications proving that the admittance technique is valid in a larger animal model. The reason this type of experiment has not yet been performed is because there are rarely situations where it is preferable to use a larger, and therefore much more expensive animal such as a dog or pig for genotype research or for large scale pharmacology trials. In order to extend the results from mice to humans, it is necessary to at least validate the admittance technique by using electromagnetic modeling.

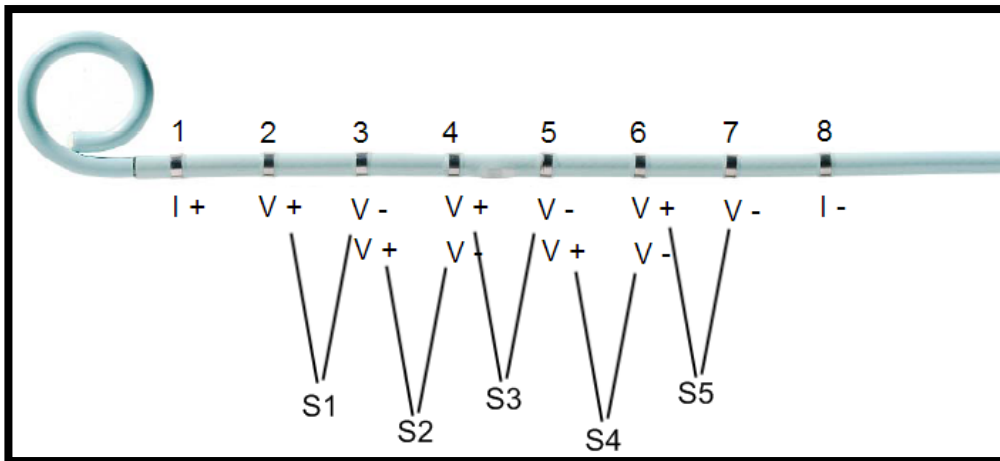


Figure 11: A Multipolar catheter with segments chosen as in Baan's first study [4].

Baan's first experiments in dogs included the use of a multipolar catheter (pictured in Figure 11) which works on the principle of superposition. This type of catheter is the most common type of catheter used in large animals because of his work

in this area. Baan suggested the use of a 5 segment measurement in the left ventricle where the total conductance, $G(t)$, could be described by the sum of all of the individual segment conductances:

$$G(t) = \sum_{n=1}^N G_n(t) + \frac{1}{3}G_1(t) \quad (18)$$

The term $G_1(t)$ in this equation is a correction factor used in Baan's experiments for the conductance missed from the space between the first stimulating electrode 1 and the first sensing electrode 2 (see Figure 11). The same current stimulating electrodes are used, but multiple voltage sensing electrodes are used in between. The voltage signal determined between each pair is then summed to determine the total conductance measured between electrodes 2 and 7. At first glance, the relation appears incorrect from a circuit analysis standpoint – conductances in series do not add. However, the relation actually sums individual volume segments, and so is correct.

The following numerical study models a 12 electrode catheter using the Finite Element Method, and explains the effects of using a larger type of catheter to make a measurement of admittance. In the previous studies in Chapter 2, a single segment is measured instead of multiple segments because only one is necessary, and in a mouse-sized heart making a multipolar catheter is challenging and expensive. Using fewer segments leads to less instrumentation, and reduces the complexity and cost of the admittance measurement system, therefore, only a single segment is modeled using the standard multipolar catheter to determine the feasibility of the measurement. A single segment also has the advantage of allowing direct comparison between previous results in mice, and results in larger animals. This study is modeled after a study previously

done in mice by Wei *et al.* [16], but using this larger catheter and more unused (floating) electrodes.

3.2 METHODS

The type of catheter modeled is a standard commercial 6 French (1.9mm diameter) 12 electrode catheter (Millar Instruments Model SPC-562-1, Houston, TX) for use in animals with a 7 mm electrode spacing. The exception is the first 3 electrodes, which are 3 mm apart, as shown in Figure 12. This catheter geometry is usually used to perform volume studies on pigs or dogs. Only 6 electrodes are shown in the model, because 6 electrodes are all that are needed to span the left ventricle, which is one of the most common places to catheterize in cardiac research. The catheter is most sensitive to changes in field geometry between the sensing electrodes, so the more proximal electrodes are omitted. Often, researchers are also interested in the left atrial volume, which explains the existence of the other electrodes. If the most distal electrode is number 1, and the electrodes are numbered consecutively, electrodes 1 and 6 are current stimulation electrodes, while electrodes 2 and 5 are for voltage sensing. Electrodes 3 and 4 are not used in this measurement, because adding the extra channels for voltage measurement requires extra instrumentation, and it is preferable to cut down the amount of instrumentation used for later miniaturization.

Even though only 4 electrodes are used in the measurement (2 for stimulation via a current source, and 2 for voltage measurement), the other electrodes are not omitted from the geometry. The walls of the cuvette are moveable to simulate a standard cuvette calibration at 0.1, 0.2, 0.5, 1, 2, 5, 10, 20, 50, 100, and 200 mL.

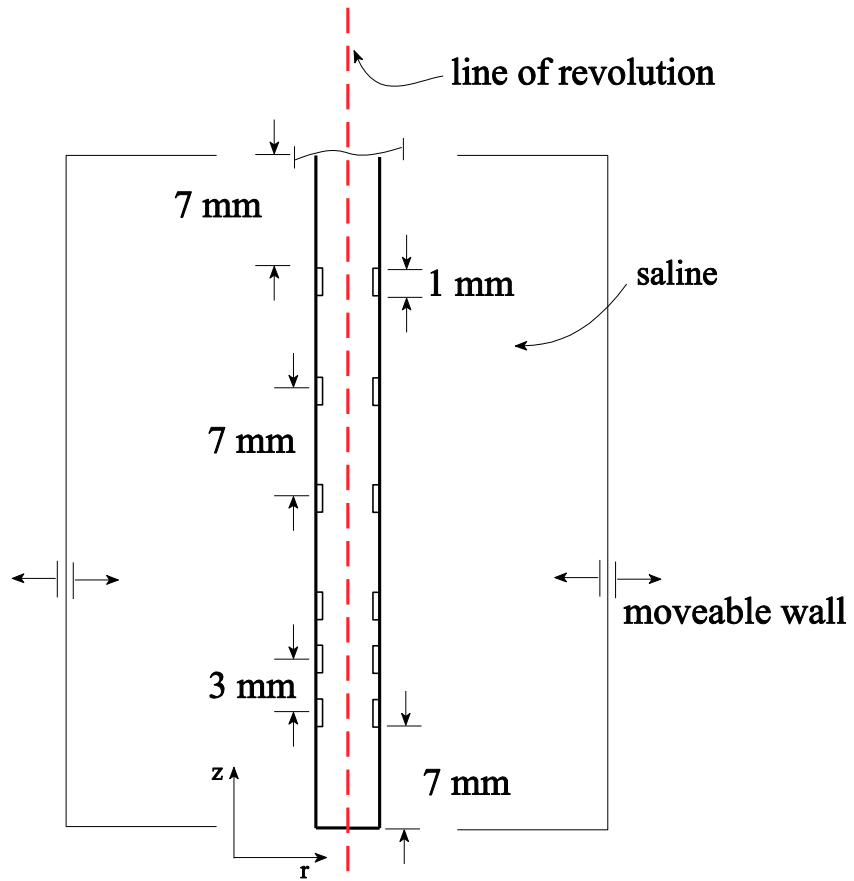


Figure 12: FEM Model 2D axisymmetric geometry; distal section of the catheter.

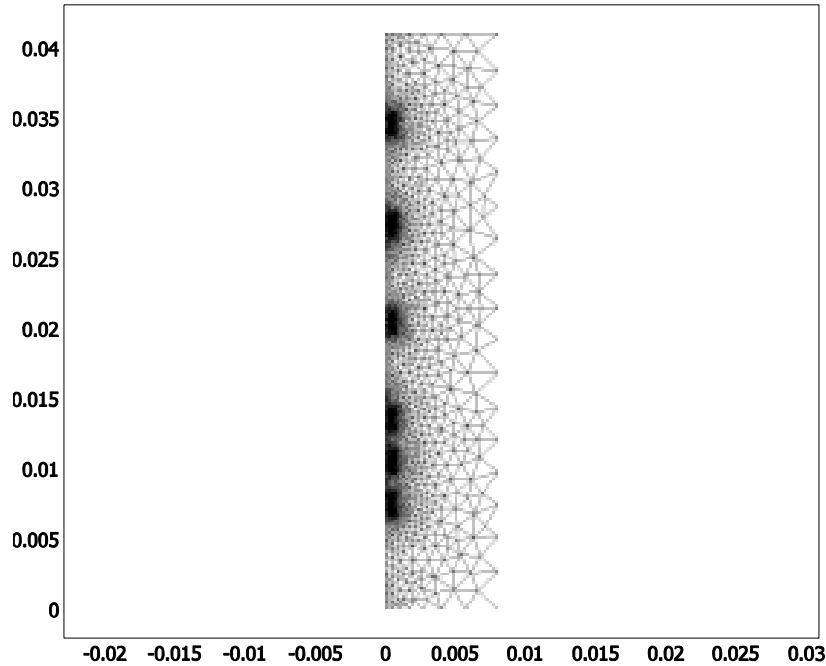


Figure 13: 2D axisymmetric mesh

The mesh shown in Figure 13 was refined near the electrodes automatically by the meshing software because of the smaller geometry present. It is also necessary to further refine the mesh near the electrodes because the area near the electrode will have the most non-uniform current density. The mesh refinement is shown in detail in Figure 14 below. The number and size of elements in the model varies based on the geometry supplied by the size of the saline container, but the minimum element quality is found in the largest cuvette, and furthest from the source electrodes of the catheter, where the current densities are greatest. All mesh parameters are summarized in Table 2.

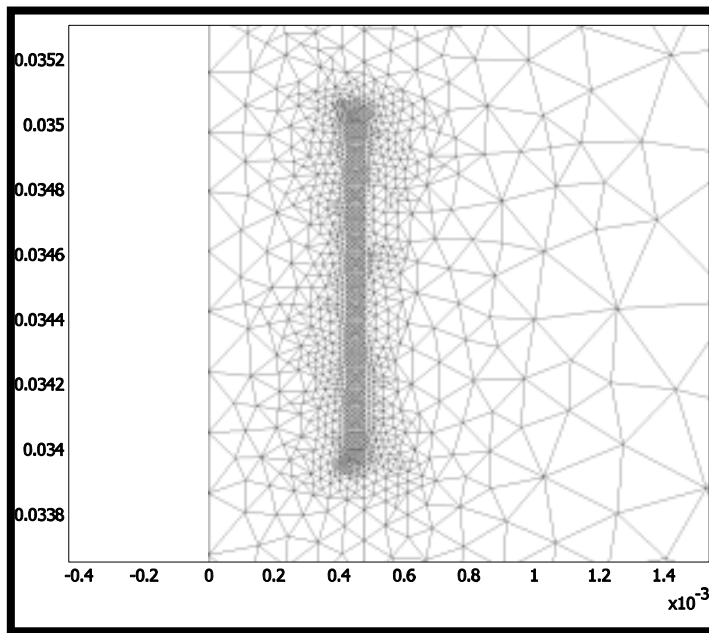


Figure 14: Closer view of one electrode, refined mesh.

Table 2: Mesh Properties

number of mesh points	5109
number of elements	10028
number of boundary elements	756
minimum element quality	0.5793
element area ratio	3.46E-05

3.3 FINITE ELEMENT MODEL (FEM) DEFINITION

The quasi-static meridional electric currents mode in Comsol is used to solve the geometry. The governing equation for this model combines Gauss' Electric Law and the Continuity Equation [11]:

$$-\nabla \cdot [(\sigma + j\omega\epsilon_r\epsilon_0)\nabla V] = 0 \quad (19)$$

where σ is the electrical conductivity (S/m), ω is the angular frequency (rad/s), ϵ_r is the relative permittivity, ϵ_0 is the permittivity of free space (F/m), and V is the electric scalar potential (V).

The electrical properties used in the model are in Table 3 below. In a cuvette, the walls of the container are normally made of plastic, which are approximated in the model as an electric insulating boundary. The catheter body is made of plastic and is placed in saline of conductivity $\sigma = 1$ S/m, which is close to the conductivity of blood.

Table 3: Electrical Properties

	σ (S/m)	ϵ (F/m)	ϵ_r
blood (37° C)	1	7.08E-10	80
normal saline (20° C)	1.6	7.08E-10	80
catheter body	0	1.95E-11	2.2
electrode	9.09E+06	8.85E-12	1

3.4 BOUNDARY CONDITIONS

The governing equation assumes the model will be submerged in an insulated space, so the boundary condition for the cuvette wall is set as an electric insulation boundary,

$$n \cdot [(\sigma + j\omega\epsilon_r\epsilon_0)\nabla V] = 0 \quad (20)$$

In the AC/DC quasi-static mode in Comsol, there are only two ways to model the electrode stimulation on the boundary. The first is as a current source by defining the current density as a constant, and then second is by defining the voltage as a constant along the boundary. Even though the stimulating electrodes are actually current sources, it is not sufficient to set the current density to a constant value. This is because by setting the current density to a single value, we are assuming that the current density will be uniform across the entire surface, which is not true because of the fringing field. Instead, the model uses an ODE setting to force the voltage to be equal to a value that minimizes the equation

$$\int \vec{J}_n \cdot d\vec{S} - I_0 = 0 \quad (21)$$

where I_0 is the desired stimulating current, while J_n is the current density flowing out of the source electrode. The integral is taken in Comsol as an integration coupling variable active only in the domain of the electrode. The result of Equation (21) is to stimulate using a current of the user's choosing (I_0), while not forcing the current density to be uniform. On the stimulating electrodes, the boundary condition is set as a voltage source, where V is forced to be a source at a frequency of 19218 Hz, close to the 20 kHz used in many commercial conductance measurement instruments. V was not forced to be exactly 20 kHz because practically speaking, it is easier to build an instrument with a frequency of stimulation that matches a common crystal oscillator frequency. In practice, the 20 kHz measurement is achieved by using a crystal oscillator with a frequency of 19218 Hz.

At the time of writing, COMSOL has introduced a new method for creating a constant current source, which ties in to the power of SPICE models. A SPICE file can now apparently be written which achieves the same effect as Equation (21).

3.5 FIELD UNIFORMITY AND ITS EFFECT ON VOLUME MEASUREMENT

The high conductivity of the electrodes that are unused in the system forces the current density to increase near the surface of the metal. This is an important point that is often overlooked in catheter measurement. Were the electrodes not present, the field would be completely uniform near the center of the catheter in a relatively small cuvette like the one in Figure 15A.

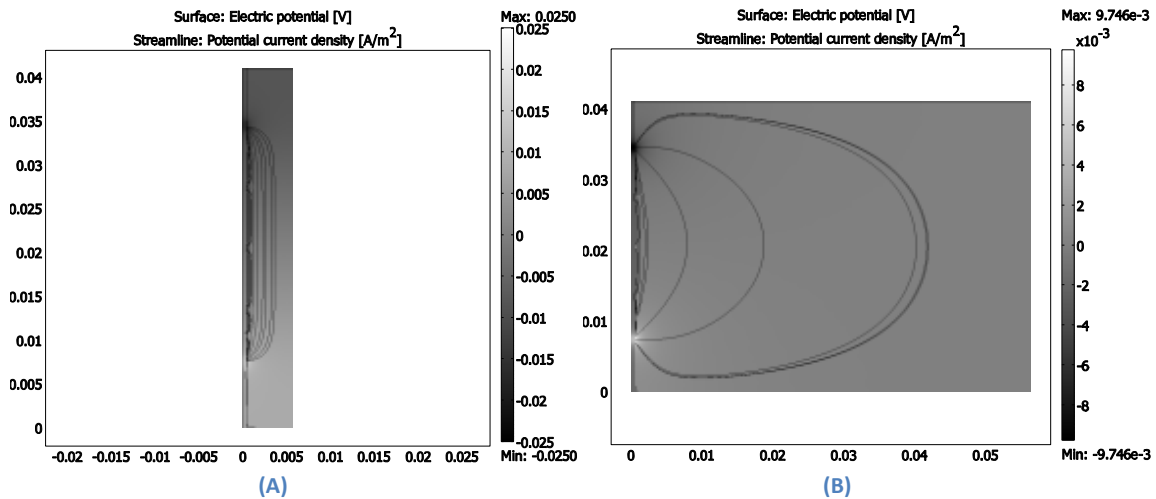


Figure 15 A: 1 mL cuvette and B: 100 mL cuvette current density (streamlines) and developed potential maps.

As seen in Figure 15A, as the volume of the cuvette measured between the voltage electrodes decreases, the uniformity of the field improves, allowing a closer estimate of true volume than in Figure 15B, where the current field spreads out to occupy the full volume of the container. This phenomenon is the reason for the nonlinear relationship between conductance and volume. The fact that there is a nonlinear relationship makes sense because as the volume of a container increases, the conductance signal measured will eventually reach a finite maximum. The point where the conductance will no longer increase even though the volume can increase is

designated G infinity, or the conductance of a volume of infinite size. This concept is illustrated with data from the model in Figure 16.

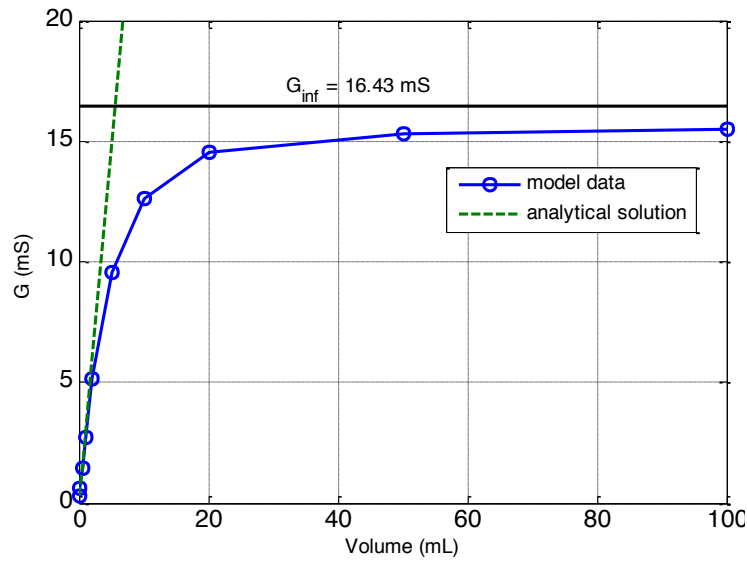


Figure 16: Nonlinearity of the Conductance-Volume Relationship in large animals

The analytical solution is calculated with a constant α , scaled to match the lower volume data. Had the unused electrodes not been present, the lower volume data would be exactly linear. The relationship between the conductance and the volume is nonlinear, which directly implies that α is nonlinear. This nonlinearity can be seen again in Figure 17, where the model results are fit to a quadratic curve. The point where $\alpha = 0$ is G infinity, and it is obvious from the linear fit that the value would be overestimated were α assumed to be linear. Some work has been done that shows that the value of alpha approaches 1 at low conductances [16, 45]. This work was done on a mouse catheter, where there were no intermediate unused electrodes. This fact, in addition to the difference in spacing between electrodes, is enough to reduce the value of α to 0.3 as G approaches 0 in these FEM model results.

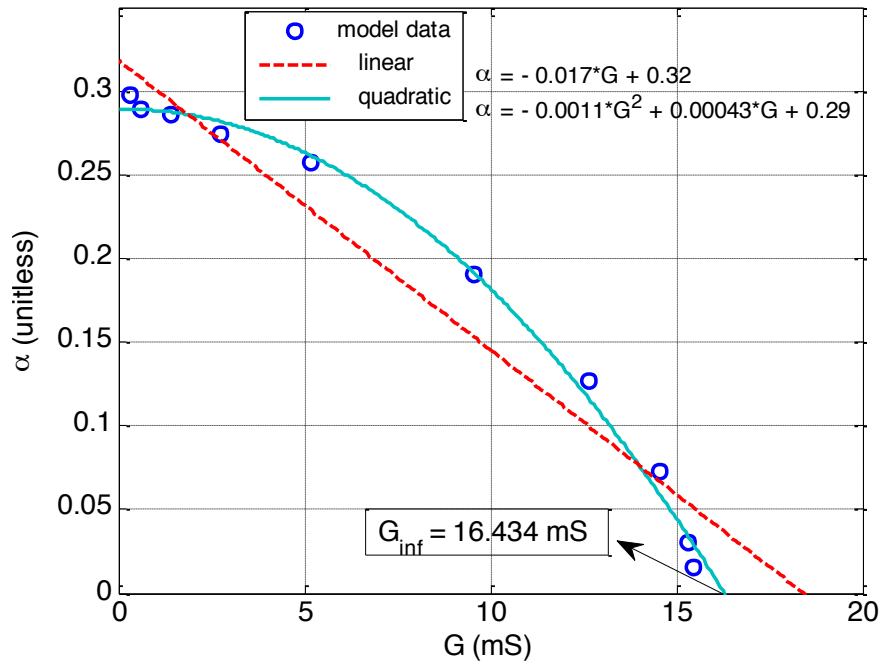


Figure 17: The Alpha – Conductance graph is nonlinear in large animals as well as in small animal model.

It is interesting to note here that many researchers still use a constant value of α in larger animal models because they are unaware that there is a nonlinear dependence to α . The effect is only less pronounced in small volumes compared to the length L from Equation (4), Baan’s Equation, because the smaller the volume relative to the size of the catheter spacing, the closer a linear relationship can approximate the true nature of α .

3.6 MODELING CONCLUSIONS

The nonlinearity of alpha is confirmed in larger animals by these results. It can be concluded from these data that it is inaccurate to use a constant or even linearly-varying value for α for any size animal, but especially so in dogs, pigs, and humans. The existence of extra unused electrodes was shown to substantially alter the current density near the catheter, and could therefore be a significant factor when interpreting results. The value of α will never equal 1 because of the effect of the unused electrodes

on the field. This is of particular importance because so many assume that at small volumes it has a value of exactly 1 (which is correct only for models with no extra electrodes). The model can be used to determine if the volume being measured is within the linear region for a given assumption of constant alpha, and also to determine whether G_{∞} is sufficiently larger than what would be measured by a given catheter design.

Chapter 4: Epicardial Preload Measurement Theory and Modeling

4.1 INTRODUCTION

The possibility of an epicardial measurement of preload is exciting clinically because of the possibility of detecting congestive heart failure much earlier than current devices. This chapter deals with the modeling and feasibility of using impedance to measure LV End Diastolic Volume (LVEDV), or preload, to detect the onset of congestive heart failure. The first section deals with the differences with the circuit model and explains why the measurement is couched in terms of an impedance measurement ($Z = \frac{1}{Y}$) instead of an admittance (Y) measurement. The second section estimates the sensitivity of this measurement to a positional placement error by the surgeon implanting a device designed to measure this impedance. Modeling using the Finite Element Method is used to estimate the error in this methodology.

4.2 CIRCUIT MODEL

An electrical model of the measurement is required to provide a means of separating the muscle component from the blood component with epicardial placement of the admittance electrodes. A traditional conductance catheter model with fixed electrodes uses a parallel combination of G_b , G_m , and $j\omega C_m$ which forms the complex admittance $\vec{Y} = G_b + G_m + j\omega C_m$ (Previously described in Chapter 2). However, the epicardial electrode placement creates the condition where the measured blood and muscle are now in series and not in parallel. Thus, a new model is developed below. For mathematical convenience, it is formulated using impedance, \vec{Z} where $\vec{Z} = 1/\vec{Y}$ (Figure 18). In the new model, the equivalents of G_b , G_m , and $j\omega C_m$ are the inverse of R_b , R_m , and $1/(j\omega C_m)$, respectively.

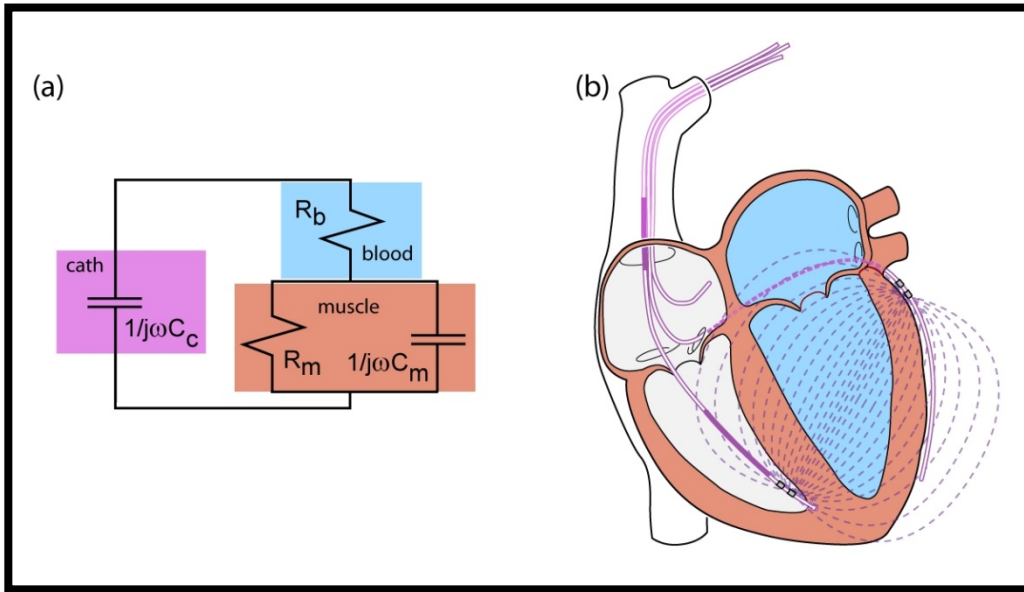


Figure 18: Epicardial circuit model (a) The electrical model of the measurement required to separate the muscle component from the blood component with epicardial placement of the admittance electrodes is shown (b) Depiction of an AICD/bi-ventricular pacemaker upon which the circuit diagram is based.

Figure 18b shows that as the stimulation current passes from an electrode placed on the LV free wall epicardium (as part of the bi-ventricular pacer), through the blood, and then through the septum, one can approximate the different layers as the boundaries between homogenous tissues of specific electrical impedance. For example, because blood does not produce a measurable phase shift at frequencies of 20kHz [33], it can be represented as a single resistance, or R_b (Figure 18a). Additionally, because muscle has both capacitance and resistance [33], it can be represented as a resistor and a capacitor in parallel, R_m , and $1/\omega C_m$, also shown in Figure 18a. The circuit model assumes that the stimulation current flows through a combination of blood and muscle in series, and capacitive and resistive properties of muscle in parallel, and is described in Equation (21). The circuit model is valid because the conductivity of blood is about 3 times higher than the conductivity of muscle, making the series path through the blood pool preferable for the majority of the current field. Because the current

passes through a muscle layer twice (LV free wall and septum), and these muscle layers are in

series, they can be represented by a single equivalent resistance and capacitance.

$$\vec{Z} = \frac{1}{j\omega C_c} \parallel \left(R_b + R_m \parallel \frac{1}{j\omega C_m} \right) \quad (22)$$

4.3 IMPEDANCE (\vec{Z}) SEPARATION OF BLOOD AND MUSCLE COMPONENTS

The derivation below demonstrates the method to derive LV volume from the epicardial admittance approach for the first time. The circuit model shown in Figure 18a can be mathematically displayed as Equation (21), where: \vec{Z} is complex impedance (Ω), R_b is blood resistance (Ω), R_m is cardiac muscle resistance (Ω), C_c is catheter capacitance (F), and C_m is cardiac muscle capacitance (F), j is $\sqrt{-1}$, and $\omega = 2\pi f$ (where f is the frequency of stimulation, 20 kHz), and \parallel means that the two quantities add in parallel, or $a \parallel b = \left(\frac{1}{a} + \frac{1}{b} \right)^{-1}$.

$$\vec{Z} = \frac{1}{j\omega C_c} \parallel \left(R_b + \frac{\frac{R_m}{j\omega C_m}}{R_m + \frac{1}{j\omega C_m}} \right) \quad (23)$$

$$= \frac{1}{j\omega C_c} \parallel \left(R_b + \frac{R_m}{j\omega R_m C_m + 1} \times \frac{1 - j\omega R_m C_m}{1 - j\omega R_m C_m} \right) \quad (24)$$

$$= \frac{1}{j\omega C_c} \parallel \left(R_b + \frac{R_m - j\omega R_m^2 C_m}{1 + (\omega R_m C_m)^2} \right) \quad (25)$$

$$= \frac{1}{j\omega C_c} \parallel \left(R_b + \frac{R_m}{1 + (\omega R_m C_m)^2} - j \frac{\omega R_m^2 C_m}{1 + (\omega R_m C_m)^2} \right) \quad (26)$$

To separate the blood and muscle components in a traditional conductance catheter tetrapolar measurement, a calibration is performed to determine the amount

of phase contribution from the catheter capacitance (C_c) for varying conductivity solutions, and remove it. However, in the epicardial Admittance measurement there is also a varying length between the current carrying electrodes that complicates the issue of calibration. For the preliminary derivation, I have assumed C_c to be small in Equation (25), allowing its impedance $1/(j\omega C_c)$ to be large in the parallel combination (and therefore neglected).

Therefore, assuming C_c to be small (high impedance), makes the parallel combination mostly dependent on the blood and tissue, Equation (25) becomes:

$$\vec{Z} \cong \left(R_b + \frac{R_m}{1 + (\omega R_m C_m)^2} - j \frac{(\omega R_m^2 C_m)}{1 + (\omega R_m C_m)^2} \right) \quad (27)$$

$$Im\{\vec{Z}\} \cong \frac{-\omega R_m^2 C_m}{1 + (\omega R_m C_m)^2} \quad (28)$$

Using the conductance / capacitance relationship in Equation (28) to separate C_m from R_m ,

$$C_m = \frac{\epsilon_m}{R_m \sigma_m} \quad (29)$$

$$Im\{\vec{Z}\} = \frac{-R_m \frac{\omega \epsilon_m}{\sigma_m}}{1 + \left(\frac{\omega \epsilon_m}{\sigma_m}\right)^2} \quad (30)$$

Rearranging,

$$R_m = \frac{-Im\{\vec{Z}\} \times \left(1 + \left(\frac{\omega \epsilon_m}{\sigma_m}\right)^2\right)}{\frac{\omega \epsilon_m}{\sigma_m}} \quad (31)$$

The imaginary part of \vec{Z} is negative because the reactance is capacitive, making R_m positive. Then,

$$R_b = Re\{\vec{Z}\} - \frac{R_m}{1 + (\omega R_m C_m)^2} \quad (32)$$

The procedure for calculating the separated blood and muscle resistances follows the derivation above.

First, a separate surface probe experiment (Figure 4, explained in Chapter 2) determines the values of σ_m and ϵ_m to use in Equation (28).

Second, the real and imaginary parts of the measurement are found using

$$Re\{\vec{Z}\} = |\vec{Z}| \times \cos(\theta) \quad (33)$$

and

$$Im\{\vec{Z}\} = |\vec{Z}| \times \sin(\theta). \quad (34)$$

Third, the results of steps 1 and 2 are used to solve for C_m , R_m , and R_b , using Equations (29), (31), and (32), respectively.

Once R_m is determined, the blood volume can be calculated directly from Baan's Equation (4), assuming that the length, L , is known. Here, the length used is the distance between the electrodes along the short axis. Obviously, this information is not available in a patient, so in preliminary results the variable α (in Baan's equation) was scaled arbitrarily to provide direct comparison of fiduciary points on the volume trace.

4.4 CONFOUNDING VARIABLES

The theory behind a normal conductance measurement explains that as the LV chamber fills with blood, the total blood resistance decreases due to the increase in the cross sectional area of blood (because of the increased blood volume). This same phenomenon should be present in the measurement of blood volume when using epicardial electrodes as well. However, there is also a variable distance between the stimulating and sensing electrodes in the impedance measurement suggested in this chapter, which will affect the impedance signal inversely. Therefore, as the length

increases between the apical and lateral electrodes, the resistance of the blood should increase, but as more blood fills the ventricle, the cross sectional area will increase, increasing the parallel pathways for current, which will cause the resistance to decrease. It is possible that because the length and the area are related, that the time-varying resistance measured may not be sensitive to volume because of counteracting effects. However, it is also quite possible that because both change as the heart beats, the effect of the change in cross sectional area could be minimized by looking at the points where the heart is largest (at end diastole). Because there is not an agreed-upon model of heart dilatation due to heart failure, this phenomenon cannot be modeled accurately without perfect information about a real heart geometry occurring during heart failure. It is therefore demonstrated experimentally in Chapter 5.

4.5 GEOMETRY OF FEM ANALYSIS

The volume of the heart can be approximated as a prolate ellipsoid if the assumption that the two short axes are equal is made. The volume of a prolate ellipsoid is defined by Equation (35):

$$Vol = \frac{1}{6}\pi A^2 B \quad (35)$$

where A is the diameter of the minor axis, and B is the diameter of the major axis. Both A and B are measured by sonomicrometry *in vivo* in Chapter 5 experiments. The geometry of the FEM solution is a 3-D model that is a simplified LV-RV chamber based on prolate ellipsoids. This geometry is used for volume computation in 2-axis echocardiographic crystal models and is used to make a rough estimate of the type of signal sensitivity expected due to surgical error in placement of the electrodes.

To determine the impact of each mm of non-ideal placement of the epicardial admittance electrodes on the final determination of LV volume, the following modeling

study was performed. Using 3-dimensional Finite Element Modeling (FEM) the measurement of impedance was analyzed in the heart shown above, using a simplified prolate ellipsoid model. Spherical electrodes of the same diameter as those on AICD/biventricular pacer leads were placed on the LV free wall (Left side of the model in Figure 19) and the right ventricular septum (Right side of the model in Figure 19). The same modeling equations as in Chapter 4 were used in COMSOL to provide a quasi-static solution for the given geometry.

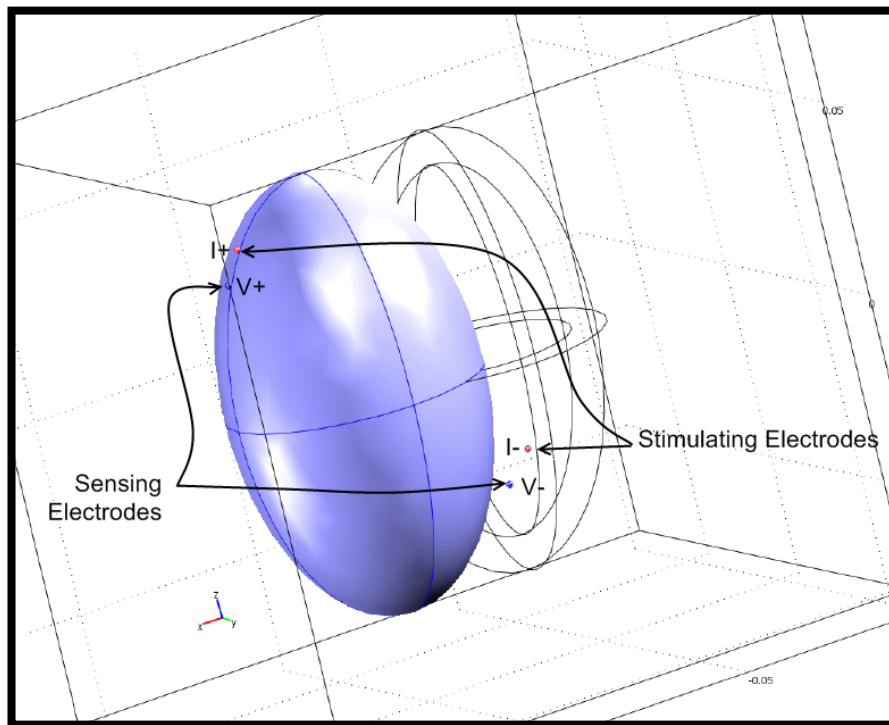


Figure 19: 3D model geometry of FEM for catheter positioning study (Posterior view of an idealized heart)

An example of the potential current density streamline plot is shown below in Figure 20.

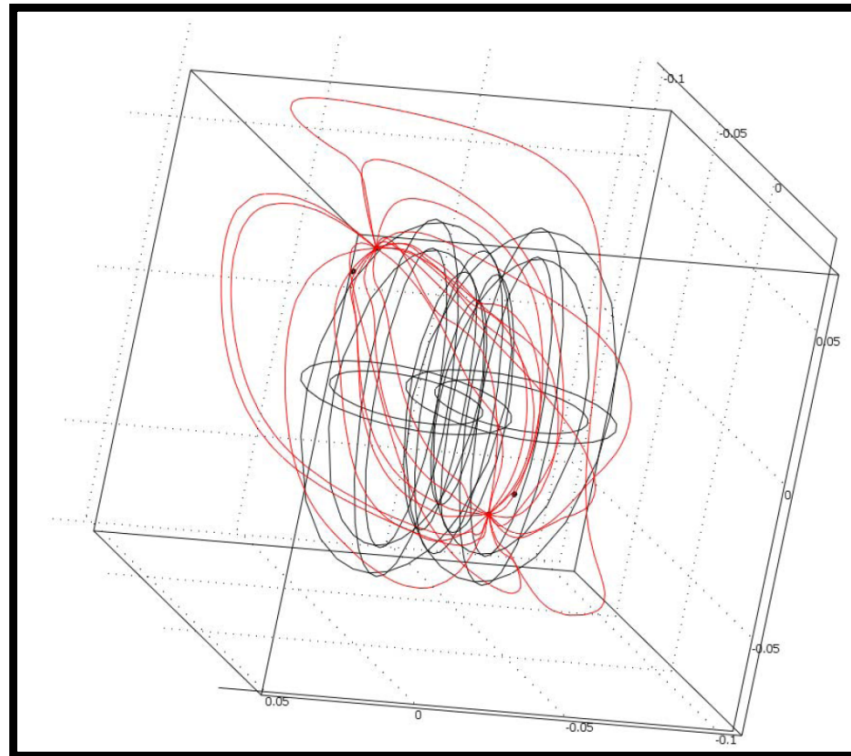


Figure 20: Potential Current Density streamline plot of FEM results

4.6 SENSITIVITY TO SURGICAL POSITIONING ERROR

The rate of success of bi-ventricular lead placement in multi-center patient studies is high, ranging between 91 to 95% in a total of 985 heart failure patients attempted [21]. Thus, technical issues related to lead placement will not be prohibitive in the long term transition of the admittance epicardial heart failure detection system to patients. Further, the coronary venous anatomies of porcine and human hearts are similar, and thus the results will be applicable to patients.

The hypothesis of this modeling study was that electrode placement at an imprecise position on the LV free wall would not significantly alter the available signal (i.e., the sensitivity to correct electrode placement is acceptably low). This was verified by fixing the RV septum leads and varying the position of the LV free wall leads on the

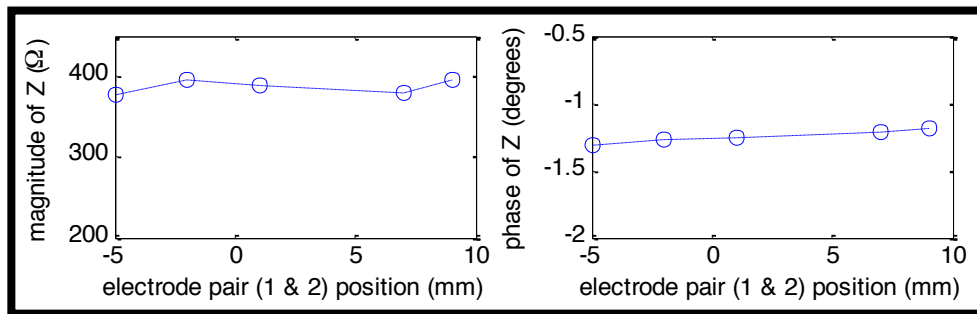


Figure 21: Results of Electrode positioning sensitivity experiment.

epicardial surface by 15 mm. The results, shown in Figure 21, demonstrate that the sensitivity to lead misplacement in the model is roughly 1% per mm for the measures of admittance (both magnitude and phase); and considerably smaller than the signal swing expected from the heart's motion between end-diastole and end-systole (approximately 40% between electrode pairs in the RV and on the LV free-wall). Therefore, it can be concluded that the error from imprecise electrode placement secondary to the sub-optimal placement of LV free wall pacing leads as dictated by coronary venous anatomy is acceptably low.

Chapter 5: Epicardial Volume *in vivo* Experiments

5.1 INTRODUCTION –ANIMAL MODEL OF CONGESTIVE HEART FAILURE

The best animal models for creating congestive heart failure in the laboratory are chronic implanted trials, but these take months to complete, which increases cost prohibitively. There are two popular models for creating heart failure in animals. The first is accomplished by inserting a pacing wire and inducing a mild tachycardia for a 1 month (or more) period of time which eventually causes the heart to decompensate. This model of heart failure is unlike the type of heart failure that occurs in humans because it does not include ischemic injury to the coronaries, as normally occurs in human heart failure. The second animal model of heart failure addresses this issue by requiring injection of microspheres over a longer period of time (1 to 2 months), which causes emboli in the coronaries, more closely resembling the cause of heart failure in humans.

There are obvious problems with both of these models of heart failure, the foremost being that the stage of heart failure induced is not easily controlled, making objective measurement of preload difficult. Additionally, proof of concept of this measurement can be done much more easily and cheaply in an acute study, which determines the feasibility of an epicardial impedance measurement as a surrogate for preload. The focus of this chapter is an acute study that shows the feasibility of an epicardial admittance measurement for the detection of volume increase. The endpoint is to justify the cost of a longer term closed chest study, which will more definitively prove that the measurement would be useful in humans.

In the study, the validity of this approach is demonstrated by: (a) detecting LV dilation with blood conductance in response to IV Neosynephrine comparable to the

standard of endocardial crystals, (b) detecting LV dilation with blood conductance in response to occlusion of the left anterior descending coronary artery, while RV pressures did not change, and (c) demonstrating that saline placed in the chest cavity to simulate pleural effusion is not a source of significant artifact in the measurement of epicardial admittance. By the conclusion of this chapter, the reader should be convinced that the admittance method outlined in Chapter 2 can be applied to moving source and sense electrodes while instantaneously removing the myocardial component to generate a final LV blood conductance signal.

5.2 METHODS

5.2.1 Calculation Theory

5.2.1.1 Epicardial Lead Blood Conductance Measurement

Tetrapolar intracardiac measurements are explained in detail in Chapter 2. Briefly, Conductance systems generate an electric field using a current source, and volume is determined from the instantaneous voltage signal that results. The most striking difference between an epicardial measurement and the traditional catheter measurement is the location of the electrodes. Conductance electrodes have not been previously placed on the LV epicardium to interrogate the LV blood volume, as has been done in the current study (Figure 22).

The relationship between measured blood conductance and LV blood volume is determined primarily by the shape of the current field in the blood pool and surrounding myocardium. In general, in a uniform electric field approximation it is seen that the measured time-dependent resistance, R_b , is proportional to the separation

distance, $L(t)$, and inversely proportional to the cross-sectional area of the field, $A(t)$;

and the converse for the measured blood conductance, G_b :

$$R_b = \frac{\rho L(t)}{A(t)}$$
$$G_b = \frac{A(t)}{\rho L(t)}$$

Some of the measurement electrode positions will produce a blood conductance primarily sensitive to the cross-sectional area change, while others are primarily sensitive to the separation distance. As the cross-sectional area of the LV increases, there is a corresponding increase in blood conductance. Thus, for the purposes of the current study, only area-dependent electrode configurations were studied.

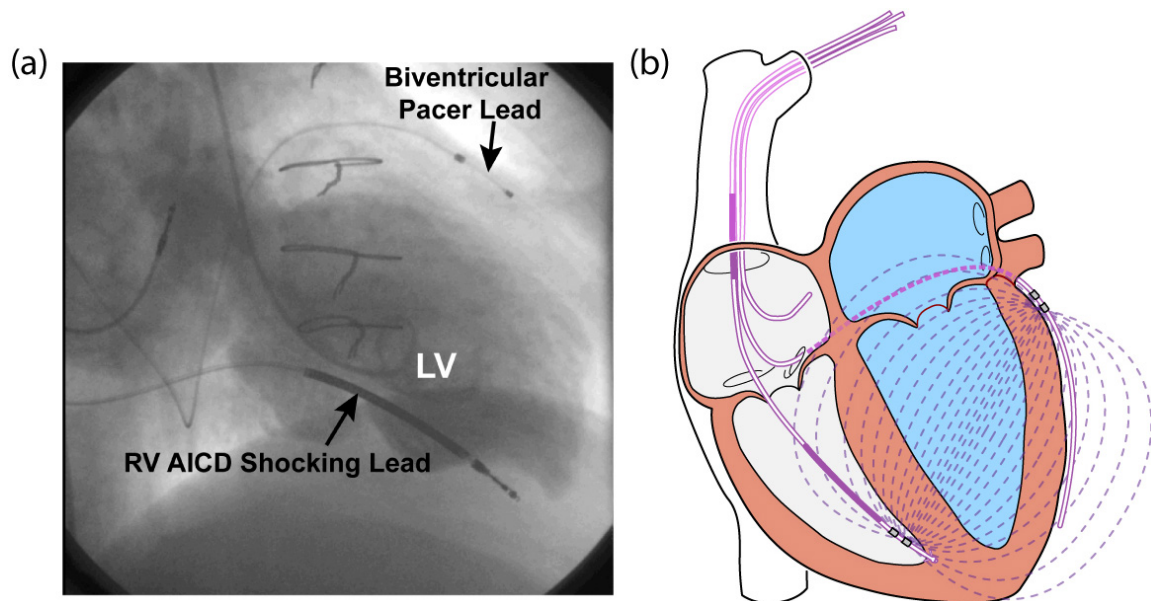


Figure 22. Pacemaker electrode positioning. (a) Bi-plane left ventriculogram from a patient with CHF and a previously implanted AICD/bi-ventricular pacer demonstrating how the leads span the left ventricle (LV) blood from the RV septum to the lateral LV epicardium. (b) The admittance electric field lines from the RV septum to the lateral LV epicardium.

5.2.1.2 Dynamic Muscle Conductance Removal

Epicardial Admittance is a measurement taken in the complex plane, and has both a magnitude, $|\vec{Y}|$ (Siemens) and a phase, $\angle \vec{Y}$ (degrees). The values for admittance are a combination of both the muscle and blood conductance, and the muscle susceptance (ωC), for both are present in the current field. The process for separating admittance into blood and muscle conductance was outlined previously for the case of a tetrapolar catheter where the blood and muscle are in parallel [17]. The method for separating blood and muscle into their constituent components follows the derivation shown in Chapter 4. These important formulae are used in the study, and are repeated below:

$$R_m = \frac{-Im\{\vec{Z}\} \times \left(1 + \left(\frac{\omega\epsilon_m}{\sigma_m}\right)^2\right)}{\frac{\omega\epsilon_m}{\sigma_m}}$$
$$R_b = Re\{\vec{Z}\} - \frac{R_m}{1 + \left(\frac{\omega\epsilon_m}{\sigma_m}\right)^2}$$

where R_m is the resistance of muscle (Ω), and R_b is the resistance of blood (Ω), ϵ_m is the permittivity of muscle (F/m), and σ_m is the conductivity of muscle (S/m). The derivations for the above formula are in Chapter 4. The complex impedance \vec{Z} can be separated into real ($Re\{\vec{Z}\}$) and imaginary parts ($Im\{\vec{Z}\}$). The properties of the myocardium σ_m and ϵ_m can be calculated using a surface probe measurement [17, 33]. In an epicardial measurement the field generated is mostly transverse, while in a surface probe measurement (and in a traditional LV catheter measurement), the field is mostly longitudinal. This difference has been measured by others, and was corrected in the

data by multiplying by a factor of 2, because longitudinal σ is 2 times larger than transverse σ [46, 47]. The penetration depth for the surface probe used to measure the porcine myocardial properties was 3.6 mm, which will not extend into the LV blood volume beneath.

5.2.1.3 LV Volume Measurement with 2 Dimensional Sonomicrometry

The standard of volume measurement used in this study was two dimensional (2D) sonomicrometry crystals. 2D sonomicrometry is an acceptable alternative in large animal hearts when the two short axes are equal in distance [31, 32, 48], and this aspect ratio is maintained during acute LV dilation. The porcine myocardium is prone to arrhythmias, and there is significant trauma associated with placing the third crystal plane through the septum. Consequently, 2D sonomicrometry is the practical approach. The two dimensions measured included the anterior-posterior and apex-base planes via pairs of 2 mm piezo-electric ultrasonic transducers positioned on the endocardial surface through a stab wound through the LV myocardium and secured with a purse-string suture. The two crystal pairs were attached to a digital sonomicrometer (Sonometrics Corporation, London, Ontario, Canada) and the digital output was then transformed into volume by fitting the points to a prolate ellipsoid [31, 32, 48].

5.2.2 Experimental Protocol

This study was conducted in compliance with the United States Food and Drug Administration (FDA) Good Laboratory Practices Regulations (21 CFR Part 58), following

approval of the animal use committee at the University of Texas Health Science Center at San Antonio. For the n = 15 Yorkshire Pigs studied, the body weight ranged from 42 kg to 78 kg (mean = 60 ± 12.6 kg), 14 were male and 1 was female. Pigs were sedated with Telazol 4 mg/kg IM, intubated and anesthesia was maintained with 1-2% Isoflurane with 100% oxygen. The right neck was dissected to gain access to the jugular vein and carotid artery. A sternotomy was performed and the pericardium was partially opened. Amiodarone, 150 mg IV, was given over 30 min, and repeated 30 min later. Following full loading of Amiodarone, a Lidocaine infusion was initiated at 1 $\mu\text{g}/\text{min}$ for the remainder of the protocol. Although there was anticipated myocardial depression from this approach, there was greater concern that the porcine model has a low ventricular fibrillation threshold. A more complete description of the protocol can be found in the Appendix.

5.2.3 Instrumentation Overview

The epicardial lead measurement protocol requires instrumentation in the following locations sewn onto the myocardial surface itself. In practice, it was found to be easier to sew the admittance electrodes to a felt backing, and then suture the felt backing to the myocardial surface, to prevent arrhythmia due to trauma on the surface of the heart from multiple stitches. The locations of all myocardial surface instruments are shown in Figure 23 below. The epicardial impedance electrodes are each spaced 1 cm apart because this is a common spacing for intraventricular catheters, and also allows for simulation of surgical error when placing the electrodes.

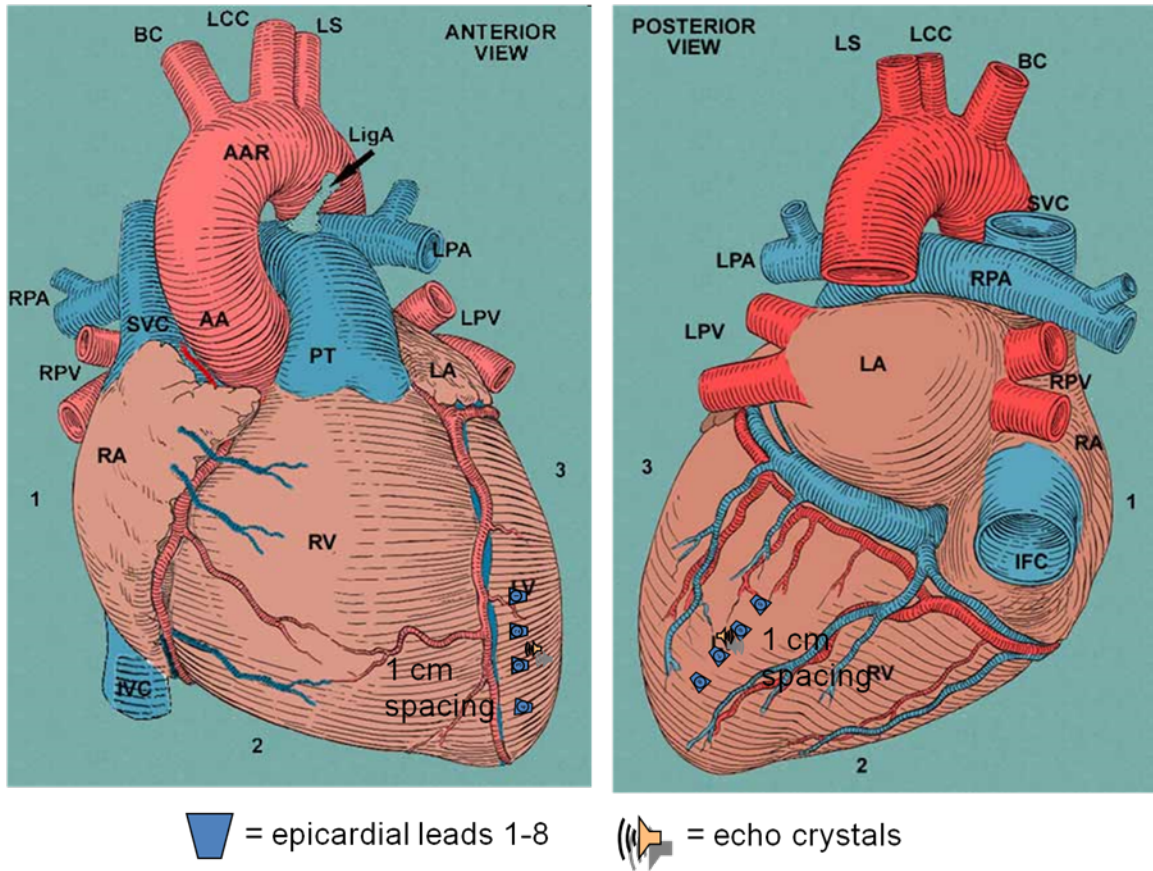


Figure 23: Detailed experimental electrode positioning. The positions of each of the 8 electrodes are represented by the trapezoids above. The sonomicrometry crystals were placed after the epicardial leads, as close as possible to the 2nd and 3rd crystal, to represent the position of the entire group as the heart beats.

Platinum-Platinum black electrodes were chosen for the experiment because of their low electrode interface impedance (Medtronic, Minneapolis, MN). Electrode locations were chosen to simulate the approximate positions of an RV AICD endocardial lead, and the bi-ventricular lead on the lateral LV epicardium. The anterior electrodes were sewn parallel to the distal LAD to simulate the RV AICD lead, and the posterior electrodes were sewn parallel to a left marginal vein to simulate the bi-ventricular pacing lead. Electrode pairs were chosen for a cross-ventricular chamber tetrapolar

measurement with a current-producing and a voltage-sensing electrode on both the anterior and the posterior epicardium. Each group of 4 possible vectors (without reflection) is referred to as a measurement “vector” in the rest of this dissertation. There are 9 vectors total, each one representing a separate measurement of impedance across the LV. In an open chest experiment, the heart sits on top of the lungs, which are expanding and contracting with each breath. Because there is no pressure from the front of the chest to keep the heart in the correct position, motion artifact is created from the lungs, which is readable in both the impedance measurement and the sonomicrometry measurements.

The pigs were also instrumented with two dimensional endocardial crystals as outlined above, a left carotid pressure sensor (3F, Scisense, London, ON), a 6F sheath in the jugular vein. A right ventricular pressure sensor was inserted directly through the anterior RV wall (1.2 F, Scisense, London, ON). A descending thoracic saline filled balloon occluder (16 or 18 mm diameter, In Vivo Metric, Healdsburg, CA) was tied around the descending thoracic aorta to generate transient occlusion as an alternative method to produce LV dilation. An aortic flow probe was placed in the descending thoracic aorta (Transonic, Ithaca, NY) immediately distal to the balloon occluder to document that occlusion was obtained.

5.2.4 Calibration

There are many possible sources of error in a measurement of admittance, including offset or gain error, which is brought on by the measurement system itself (discussed in Section 5.2.4.1), and error from the electrode-electrolyte interface effects (discussed for each probe individually in Sections 5.2.4.2, and 5.2.5). These sources of error must be accounted for in order to make an accurate measurement.

5.2.4.1 Admittance Instrument Calibration

A 5-segment multiple gain conductance measurement system called a GX5 (Scisense, London, ON) was retrofitted with a 5-segment phase measurement system by Erik Larson to create a 5 channel admittance measurement system. In order to ensure proper functionality, the input of this system was attached to a potentiometer and capacitor and the total impedance was varied over the range of the real and imaginary planes of measurement. These were then checked against the theoretical admittance which would be produced by each RC load, to make sure that no significant error is introduced by the system itself. In the GX5 system, the error introduced by the system is minimal.

5.2.4.2 LV Epicardial Lead Calibration

There is no offset present in the measurement because of the system itself. At the point where previous step (5.2.4.1) is complete, the measurement is essentially calibrated out to the plane of the input terminals to the GX5. However, there is still the effect of the electrodes and electrode/electrolyte interface to consider. Because the assumption of the impedance separation equations (Equations 30 and 31) is that the electrode capacitance is negligible, this assumption was tested before each experiment.

In order to check this assumption, the electrodes were submerged in saline of conductivity $\sigma = .8 \text{ S/m}$ and the output of the GX5 is checked for a phase angle shift (indicating measurable capacitance from the electrodes or the electrode/electrolyte interface effect). The conductivity of pig blood averages around this value of conductivity, and saline was used because it does not introduce a phase shift in an impedance measurement ($\epsilon_r \approx 80$, the same as water). Because all complex impedance in this system must be capacitive, and because the electrodes never produce more than 1 degree of phase shift on the output, regardless of orientation, they do not require calibration beyond this point in the study. Ideally, the catheter and the instrument should not contribute to the measured phase in an experiment. The best known methods for removing their contribution is outlined in Chapter 2.

5.2.5 Surface Probe Calibration

The biggest difference between a pig probe and the previous mouse probe is, of course, the size. The length between the current stimulating electrodes on the surface probe determines the penetration depth of the measurement field, and this electrode is designed for a deeper penetration because the pig LV myocardium is roughly 1 cm thick. This larger spacing also reduces the amount of interwire capacitance in the probe, which increases the standard deviation of muscle properties over that observed in a mouse measurement.

The surface probe is calibrated exactly as the surface probe is calibrated in the mouse study in Chapter 2. Saline solutions of conductivity $\sigma = 2000, 4000, 6000, 8000,$ and $10000 \mu\text{S/cm}$ span the range of conductivities necessary to measure myocardial properties, and the phase offset due to the surface probe is recorded after

measurement on the surface of these 5 solutions. This phase offset is then removed from the measurement by subtracting the probe's contribution to the susceptance.

5.2.6 Properties Measurement and Hematocrit

A custom-designed epicardial probe was applied to the surface of the intact beating open-chest heart of all $n = 15$ pigs studied (for calibration see Section 5.2.5). The technique used is similar to the technique used in the mouse experiments in Chapter 2. The pig anatomy is large enough that an area of the muscle that is devoid of blood vessels is easily found. This is usually an area near the placement of the anterior electrodes, but lateral to the Left Anterior Descending Artery. $N=3$ measurements are taken in two positions that are perpendicular to each other on a large patch of myocardium (not over a coronary blood vessel), to ensure that myocardial properties do not change with probe orientation. These measurements are retaken before each procedure in the protocol because any extended period of surgery can cause noticeable changes in the health and hydration of the myocardium. These measurements are taken to ensure that the preparation is not compromised because of changing physiologic conditions.

The measurement current was generated using the instrumentation previously described [9]. Real-time $|Y|$ and θ were measured and myocardial permittivity (ϵ_m) and conductivity (σ_m) were calculated as described previously [33]. Briefly, the surface probe "cell constant", k (m^{-1}), determined in saline of known electrical conductivity, is used to calculate: $\sigma_m = k \times G_m$ and $\epsilon_m = k \times C_m$, where $G_m = Re\{\vec{Y}\}$ and $C_m = Im\{\vec{Y}\} / \omega$ and $\omega = 2\pi f$, where k is the cell constant of the probe used ($1/m$), G_m is the conductance

of muscle (S), C_m is the capacitance of the muscle, and f is the frequency of measurement (Hz). Hematocrit was determined both at baseline and at the end of the experiment via capillary tubes and a Clay Adams Readacrit centrifuge (model CT-3400, Becton Dickinson & Company, Sparks, MD). Whole blood samples were spun for 5 minutes at 8,500 rpm, and the volume of packed red cells was expressed as a percentage of total volume.

5.2.7 Neosynephrine (Phenylephrine) for LV dilatation

Neosynephrine was chosen to increase afterload and secondarily dilate the LV in a dose-response fashion to simulate LV dilation as would occur in a heart failure patient. Neosynephrine was infused at constant flow rates of 75, 150, and 300 $\mu\text{g}/\text{min}$ in the first $n=2$ pigs. For the later $n=9$ pigs, a lower dose of 37.5 $\mu\text{g}/\text{min}$ was added to this infusion protocol. Baseline and data from at least 2 doses of Neosynephrine where LV dilation occurred, as defined by endocardial crystals, were required for data analysis. Some doses of Neosynephrine did not result in LV dilation and this varied in every pig. Thus, the doses given in the results section are the baseline, and mean low and high doses of Neosynephrine that achieved LV dilation, as defined by endocardial crystals. Each dose of Neosynephrine was infused for 10 minutes to achieve steady state, and then data were acquired over the subsequent 5 minutes for a total of 15 minutes per dose.

Data acquired at baseline and at each dose of Neosynephrine included heart rate, carotid pressure (AoP), descending thoracic aortic flow (Ao Flow), short and long axis

endocardial crystals, epicardial impedance magnitude ($|\vec{Z}|$) and phase angle ($\angle \vec{Z}$).

Data were acquired while the respirator was suspended at end-expiration for at least 5 cardiac cycles.

5.2.8 Alternative methods for LV dilation

To determine if LV dilation could be detected by epicardial admittance preceding increases in right ventricular pressures, two additional preparations were examined – acute LAD occlusion and transient aortic occlusion. The question could not be posed in the Neosynephrine dose-response study because this medication acts as an α_2 receptor agonist, and this receptor is present in both the systemic and pulmonary vasculature. Thus, it was not possible to obtain an isolated increase in LV afterload without a simultaneous increase in RV afterload [49, 50] using Neosynephrine.

5.2.8.1 LAD occlusion

A suture was placed under the middle LAD, above the level of the epicardial admittance electrodes, and tied off to produce an acute dilation of the middle and distal anterior myocardium. Data obtained were identical to the Neosynephrine protocol, but right ventricular pressure was also measured. Due to ventricular fibrillation, complete data was only obtained in n=6 experiments.

5.2.8.2 Transient Aortic Occlusion

Transient aortic occlusions were needed to supplement the Neosynephrine because they are a “purer” method of volume increase. One cannot use the occlusions

as a steady state intervention because reflex changes in the heart do not allow the heart to reach steady state for any length of time.

Transient aortic occlusion was performed successfully in $n = 11$ pigs. Occlusion was controlled by a water filled balloon occluder, sutured around the descending thoracic aorta and inflated slowly until the LV end-systolic pressure (measured from the Aortic Pressure tracing) reaches roughly 150% of its baseline value. Successful occlusion was defined by an average descending thoracic aorta flow of less than 1 L/min. This briefly causes the volume to increase, and at the same time, measurements are taken as in the previous protocol. The flow probe was always located immediately distal to the balloon occluder to quantify the degree of ligation.

5.2.9 Pleural Effusion Simulation

Pleural effusions are common in heart failure patients, and are a common source of artifact in the measurement of lung conductance by systems such as Optivol™ [25, 26, 28] and CorVue™ since the electric field generated by these devices extends into the lungs. Epicardial admittance generates an electric field that extends across the LV and thus should not include this artifact. To test this hypothesis, the chest cavity was filled with saline during the measurement of epicardial admittance. The animal model in this study is not a model of chronic heart failure, therefore a real pleural effusion cannot be produced. The pericardium was used as a sling to keep the saline from coming into direct contact with the electrodes, similar to the final implementation of epicardial admittance. Immediately after baseline measurements as outlined above, saline of

conductivity close to that of blood ($7941 \pm 124 \mu\text{S}/\text{cm}$) was introduced into the chest until respiration nearly caused the saline to spill into the pericardial sack. This volume for $n = 7$ pigs was 425 ± 90 mL, and following introduction all measurements were repeated.

5.2.10 Data Analysis

The slope relating blood conductance (mS) and endocardial crystal volume (mL) was determined in 11 animals at up to three doses of neosynephrine in each of up to 6 vectors, yielding a total of 99 paired measures of blood conductance and crystal volume (Figure 23). Data were analyzed based on a repeated measures linear model with a compound symmetric autocorrelation matrix and fixed intercepts for each pig and vector. The significance of the relation between blood conductance and crystal volume was assessed using a Wald statistic for testing the null hypothesis that the coefficient of LV blood conductance in the repeated measures linear model is zero. Statistical testing was two-sided with a significance level of 5% using SAS Version 9.2 for Windows (SAS Institute, Cary, North Carolina). For LAD occlusion, transient Ao occlusion, and pleural effusion simulation, paired baseline and intervention data was compared using a Student's t test, again with a level of significance of 5%. All results are reported as mean \pm standard deviation.

5.3 RESULTS

5.3.1 Baseline Hemodynamics

The mean peak aortic pressure was 80 ± 13 mmHg, and the heart rate was 86 ± 17 bpm. The mean LV end diastolic and end systolic long axis dimensions by crystals were 82 ± 6 and 74 ± 5 cm, respectively; and the mean LV end diastolic and end systolic short axis distance by crystals were 47 ± 4 and 40 ± 4 cm, respectively. The calculated mean LV EDV was 100 ± 31 mL, and the mean LV ESV was 69 ± 25 mL measured via sonomicrometry. The mean EF was $31 \pm 6\%$, consistent with a depressed but non-dilated LV preparation from the amiodarone and anesthetics given to minimize ventricular fibrillation. The mean descending thoracic aorta flow was 8.0 ± 1.8 L/min, and the mean RV systolic pressure was 19 ± 3 mm Hg.

Hematocrit at the initiation of the protocol was $30 \pm 2.3\%$, and at the end of the protocol $33 \pm 4.7\%$, consistent with hemo-concentration due to minimal fluid administration during the protocol to mitigate against changes in blood and myocardial electrical properties as a source of artifact. The mean distance from the LV apex to the most apical epicardial admittance electrode on the anterior surface was 3.0 ± 0.9 cm, and on the posterior surface was 3.0 ± 0.5 cm, consistent with the admittance electrodes being parallel to one another on either side of the LV epicardium.

The end diastolic and end systolic epicardial LV admittance magnitude ($|\vec{Y}| = 1/|\vec{Z}|$) were 15.8 ± 2.0 and 14.5 ± 1.9 mS, respectively; and the mean phase angle ($\angle \vec{Y} = -\angle \vec{Z}$) were 9.2 ± 3.0 and 7.4 ± 3.21 degrees, respectively.

5.3.2 Properties summary

The properties of myocardium were determined in each pig for use in the equations to separate the blood and muscle admittance as described previously [33]. In the $n = 15$ pigs studied, the myocardial conductivity was $\sigma_m = 0.33 \pm 0.03$ S/m, the myocardial permittivity was $\epsilon_m = (19710 \pm 2786) \cdot \epsilon_0$ F/m, and the calculated ratio of σ/ϵ for myocardium was $1,923,320 \pm 179,592$ S/F.

5.3.3 Neosynephrine for LV dilatation

Neosynephrine is a positive inotrope that increases afterload by increasing the pressure in the heart. There is not much published literature which supports the use of Neosynephrine to increase the volume of a pig LV, and this is because most drugs are not given for the purpose of inducing heart failure. Neosynephrine affects the afterload of the heart only during the time it is being infused, and it took roughly 20 minutes for the pigs in our study for the effect of Neosynephrine to wear off (i.e. for the baseline pressure to be achieved). Neosynephrine is also given at a lower dose (10-25 $\mu\text{g}/\text{min}$) to keep the pressures high for survivability early in the surgical preparation, so this dosage was stopped 20 minutes before the first baseline for this study was performed.

Example data are shown in Figure 24, which also demonstrates how the short and long axis crystals were used to derive the standard for LV volume (LV Crystal Vol), and that epicardial impedance ($|\vec{Z}|$) and phase angle ($\angle\vec{Z}$) were used to derive LV blood conductance.

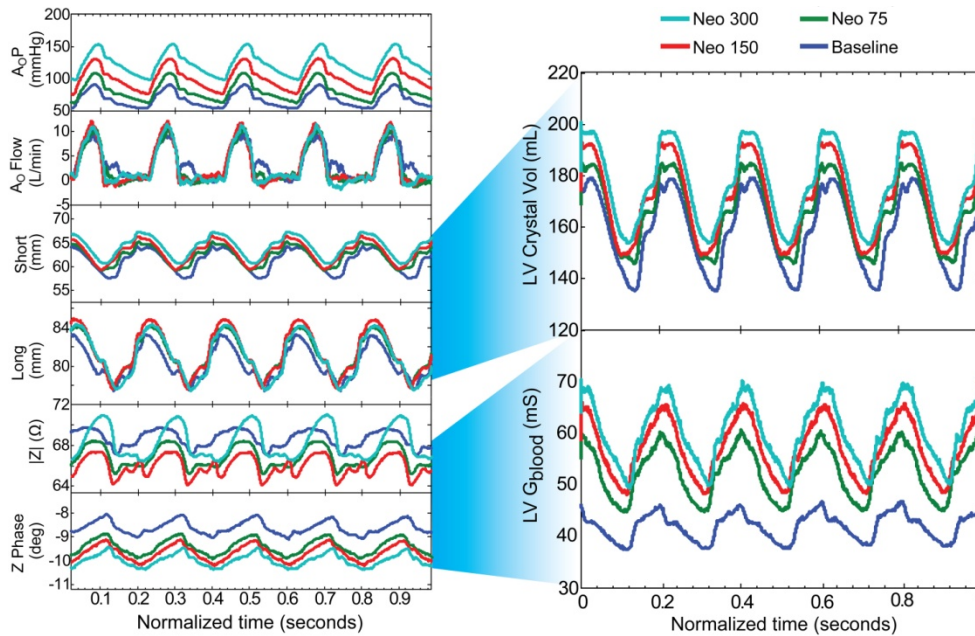


Figure 24. Typical Neosynephrine dose-response (Neo D-R) data obtained from a single porcine study which demonstrates the raw signals, and which signals are used to derive final LV blood conductance (LV Gblood). The Ao pressure increased with the Neo D-R, while aortic flow was constant. Both short and long axis LV endocardial crystals increased in distance with Neo D-R, as did calculated LV volume (LV Crystal Vol, mL). The epicardial impedance ($|Z|$) and phase angle (Z Phase) also changed in response to the Neo D-R, as did calculated LV Gblood (mS), with greater sensitivity (see Figure 23) than the LV volume standard.

Data from all porcine studies are shown in Figure 25. For data to be included in this figure, at least $n=2$ doses of Neosynephrine (Neo) were administered that resulted in LV dilation as defined by endocardial crystals. The low dose Neo was $90 \pm 54 \mu\text{g}/\text{min}$, the high dose Neo was $180 \pm 107 \mu\text{g}/\text{min}$. The blood conductance was computed from the epicardial impedance ($|\vec{Z}|$) and phase angle ($\angle\vec{Z}$), and plotted against LV volume

calculated from endocardial crystals. As is apparent from the figure, a dose-dependent relationship was obtained for multiple electrode locations in multiple animals. The conductance of blood (G_b), expressed in milli-Siemens (mS), and left ventricular volume (V), expressed in milliliters (mL), were measured at multiple values of LV volume using between 1 and 6 vectors on each pig and the within-animal mean slope was computed. The slope relating G_b (mS) and the adjusted volume (mL), 1.16 ± 0.48 ms/mL, was significantly different from zero ($p=0.017$).

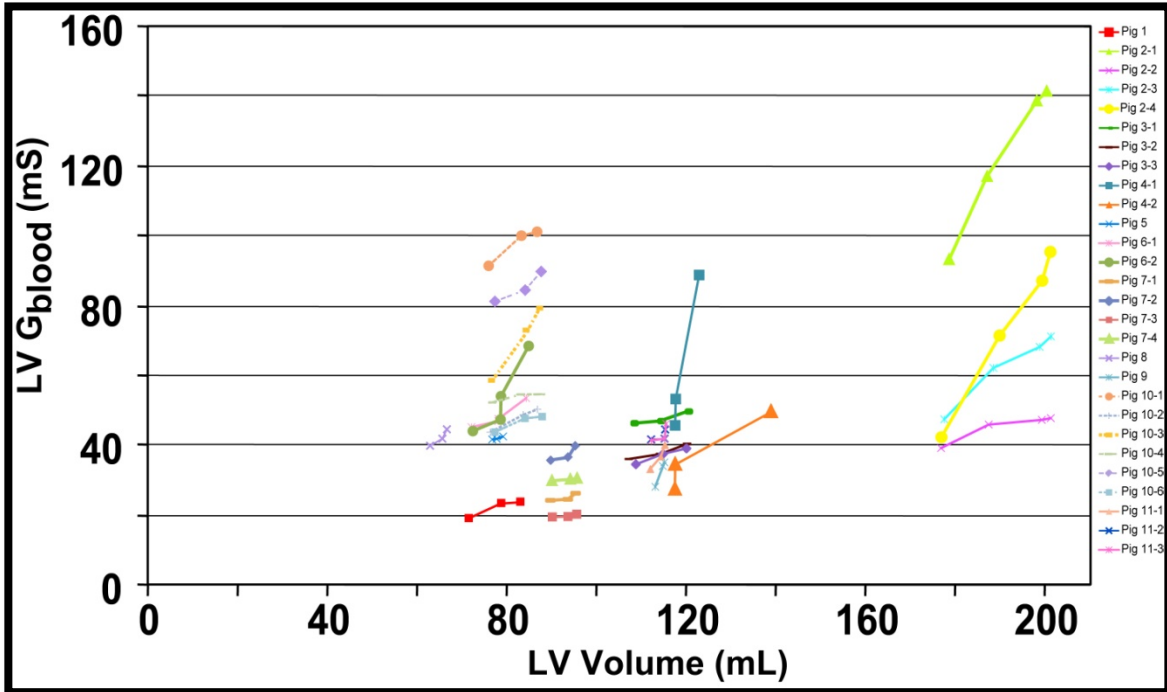


Figure 25. Demonstration that blood conductance, G_b , determined from epicardial admittance, detects LV dilation in response to Neosynephrine dose-response (see text for greater detail). The pig number and electrode pair are identified in the legend.

5.3.3.1 LAD Occlusion for LV Dilatation

Hemodynamic parameters are shown in Table 4 at baseline and following LAD occlusion.

Table 4. LAD Occlusion. Data from n=6 pigs with 13 electrode positions are shown. HR is heart rate, AoP is systolic right carotid pressure, Echo Vol is 2D endocardial crystal LV volume, Ao Flow is descending thoracic aortic flow, RVSP is right ventricular systolic pressure, and G_{blood} is LV blood conductance derived from epicardial admittance. ‡ p < 0.01

LAD Occlusion (n = 6 pigs, 13 electrode positions, 2 per pig)

	Baseline	Occlusion	Difference
HR (bpm)	87.7 ± 18.5	87.4 ± 20.2	-0.2 ± 4.2
AoP (mmHg)	88.3 ± 9.2	82.8 ± 11.1	-5.6 ± 5.2 ‡
Echo Vol(mL)	87.7 ± 11.5	91.3 ± 12.2	3.5 ± 2.0 ‡
Ao Flow (L/min)	7 ± 1.3	6.4 ± 1.3	-0.6 ± 0.5 ‡
RVSP (mmHg)	24.5 ± 3.9	23.7 ± 5	-0.8 ± 1.5
G blood (mS)	73.6 ± 39.8	85 ± 51.1	11.4 ± 12.8 ‡

Acute LAD occlusion produced a significant decrease in aortic pressure and flow. The anticipated increase in LV volume was detected by both the volume standard (endocardial crystals) and blood conductance. The large standard deviations in the blood conductance are a result of the wide range of electrode positions and offset, which may be caused by contact resistance in the surface electrode geometry. On average, an increase of 17% from baseline LV blood conductance can be expected to correspond to an LV volume increase of 4%.

5.3.3.2 Transient Ao Occlusion

Hemodynamic parameters are shown in Table 5 at baseline and peak transient Ao occlusion.

Table 5. Ao Occlusion Data from n=11 pigs from 27 electrode positions are shown. Occlusion data was defined at the time of peak AoP. HR is heart rate, AoP is systolic right carotid pressure, Echo Vol is 2D endocardial crystal LV volume, Ao Flow is descending thoracic aortic flow, RVSP is right ventricular systolic pressure, and G_{blood} is LV blood conductance derived from epicardial admittance. ‡ $p < 0.01$

Aortic Occlusion (n = 11 pigs, 27 electrode positions, 2 per pig)

	Baseline	Occlusion	Difference
HR (bpm)	90.1 ± 28.4	97 ± 23.7	6.9 ± 28.1
AoP (mmHg)	86.1 ± 10.9	123.5 ± 17.5	37.4 ± 9.9 ‡
Echo Vol(mL)	88.7 ± 20.5	97.8 ± 21.8	9.1 ± 4.6 ‡
Ao Flow (L/min)	6.3 ± 1.2	0.7 ± 0.6	-5.6 ± 1.1 ‡
RVSP (mmHg)	22.9 ± 4.4	23.8 ± 4.4	0.9 ± 0.7 ‡
G blood (mS)	53.5 ± 18.6	57.4 ± 21.6	3.9 ± 4.3 ‡

HR decreases, while AoP and the crystal derived LV volume all increase. Ao flow decreased below 1 L/min since that was the definition for a successful aortic occlusion.

The increased afterload increases the crystal volume by an average of 9%, and the blood conductance increases similarly by 7%. RV systolic pressure also increased slightly.

5.3.3.3 Pleural Effusion Simulation

Hemodynamic parameters are shown in Table 6 at baseline and pleural effusion simulation. The LV blood conductance did not change with saline placed around the heart, nor did the crystal derived LV volume.

Table 6. Pleural Effusion Simulation. Data from n=7 pigs from 54 electrode positions are shown. HR is heart rate, AoP is systolic right carotid pressure, Echo Vol is 2D endocardial crystal LV volume, and G_{blood} is LV blood conductance derived from epicardial admittance. † $p < 0.05$, ‡ $p < 0.01$

Pleural Effusion Simulation (n = 7 pigs, 54 electrode configurations, 7 per pig)			
	Baseline	Pleural Effusion	Difference
HR (bpm)	95.2 ± 19.0	96.1 ± 20.6	0.8 ± 2.6 †
AoP (mmHg)	87.4 ± 4.9	86.1 ± 5.9	-1.3 ± 3.4 ‡
Echo Vol(mL)	100.0 ± 28.5	100.2 ± 27.4	0.1 ± 2.6
G blood (mS)	53.2 ± 33.5	52.6 ± 27.8	-0.5 ± 18.9

5.4 DISCUSSION

This study has demonstrated that LV blood conductance can be successfully estimated from the epicardial position, despite the current generating and sensing electrodes being in constant motion with the heart, and with dynamic removal of the myocardial component of the returning voltage signal. Specifically, it has been demonstrated that: (a) a physiologic LV blood conductance signal can be derived, (b) LV dilation in response to dose-response iv Neosynephrine can be detected by blood conductance in a similar fashion to the standard of endocardial crystals, (c) the physiologic impact of acute LAD occlusion can be detected by blood conductance as LV dilation, but not as a secondary rise in RV systolic pressure, and (d) pleural effusions simulated by placing saline outside the pericardium did not serve as a source of artifact for blood conductance measurements.

The blood and myocardium affect the electric field generated from the epicardial electrode position differently than in the traditional intra-ventricular fixed electrode catheter measurement. In the epicardial lead configuration, the field travels completely

through the entire thickness of the myocardial wall on both sides of the LV, while in an intra-ventricular configuration, only a part of the field enters the myocardium (i.e., traditional parallel conductance). This dictates the evolution of unique circuit models to explain the new electrode positions. The real part of the impedance $|\vec{Z}|$ (more commonly known by its inverse, traditional conductance), is used to determine LV volume from the intra-ventricular position by creating a circuit model of the blood and muscle resistance in parallel. The traditional approach has not included the capacitance of the myocardium, introduced by the admittance approach laid out in Chapter 2. In contrast, the circuit model used in the epicardial approach introduced in the current study is more complex (see Chapter 4). The capacitive component of the myocardium is in parallel with the muscle resistance. Further, the blood resistance is now in series with the parallel muscle resistive and capacitive components, leading to different equations for dynamic separation of blood and muscle components.

Right sided pressures (RV, RA) are used in many implanted devices to predict future episodes of heart failure in patients [22, 24, 51]. The backwards heart failure theory[18] argues that heart failure initiates in the LV in these patients, and subsequently elevates left atrial pressure, resulting in pulmonary edema, and finally elevates right sided pressures, all downstream from LV volume or preload and hence less sensitive measures of future heart failure episodes. This theory is best tested in a chronic heart failure model since LV diastolic compliance is increased by this condition,

and hence a greater change in LV volume will produce a less robust elevation of right sided pressures. Despite the study being an acute preparation examining normal sized LVs (despite depression of ventricular function by amiodarone and anesthetics), acute LAD occlusion was able to confirm this theory by demonstrating an elevation of both LV blood conductance and echo crystal volume but no increase in RV systolic pressures. These results are consistent with the hypothesis that an increasing LV blood conductance will be a more sensitive indicator of impending future episodes of heart failure than alternative upstream pressure and lung conductance approaches.

Pleural effusions are frequent findings in patients with advanced heart failure. Devices that interrogate the lungs for pulmonary edema use a trans-thoracic resistance measurement from the tip of the RV AICD lead to the case of the battery pack for the pacemaker/defibrillator, and thus provide a wide electric field including the LV, left atrium, thoracic skeletal muscle, ipsilateral lung tissue, intravascular blood volume in the lung, pulmonary interstitial edema and finally pleural effusions to measure a changing fluid index. Having an electrical approach that is focused on the LV myocardium and blood volume would be preferable, but still has some electric field extension into other sources of artifact such as pleural effusions. To determine whether epicardial admittance will artifactually detect pleural effusion, fluid was placed outside the pericardium in the chest cavity to simulate this clinical condition. No alteration in the measurement of LV blood conductance occurred in these studies, arguing that epicardial admittance does indeed focus its interrogation on the LV itself.

There are several limitations in this study. First, although an increase in LV volume could be distinguished from an increase in RV systolic pressure with Ao occlusion, this pressure increase was not present in the LAD occlusion study. However, while RV systolic pressure increase was statistically significant, the absolute mean increase was 0.9 mm Hg, which is not clinically significant. It was not possible to use Neosynephrine infusion to test the theory that LV preload will be a more sensitive indicator of impending heart failure than right sided pressures since both the systemic and pulmonary circuits have α_2 receptors [49, 50]. Ultimately, this hypothesis is best tested in a dilated LV where reduced chamber compliance will further favor LV preload as being the most sensitive endpoint for impending heart failure. Second, the admittance electrodes were not placed onto ACID and bi-ventricular pacing leads deployed in their appropriate locations. However, as the transition is made to this next preparation during future chronic studies, improved admittance electrode contact is anticipated, which was a source of error in the current study due to air acting as an insulator between the electrode – myocardial interface in the open chest porcine preparation employed. Finally, LV blood conductance was not converted to LV volume. Baan's equation [4, 12] is not applicable since L is not a constant. Future studies will require derivation of a new blood conductance to LV volume equation.

In conclusion, a new electrical approach to impending heart failure detection has been developed, taking advantage of pre-existing AICD and bi-ventricular pacing lead locations, and maturing the conductance approach to moving source and sensing

electrodes while instantaneously removing the myocardial component to generate a final LV blood conductance signal.

Chapter 6: Conclusion and Future Work

6.1 FUTURE WORK

The methodology for determining LV preload using an epicardial admittance measurement in large animals has been shown using acute studies in this dissertation. To apply this measurement to humans for use in detecting heart failure, more work needs to be done. First, heart remodeling happens over the course of weeks (if not months) and not in an acute setting, which occurs in minutes. The possibility of long term measurement of heart remodeling remains a question, and a new animal model may be needed for long term implantation and testing. Secondly, the length vs. area effect on measured conductance is still not completely understood and a method for converting the admittance to a calibrated volume is not forthcoming. This problem is less important because blood conductance has already been shown to be well correlated with volume increase. Finding the electrode placement with the greatest long-term change may be affected by other variables as well such as changing electrode impedance over time, tissue necrosis causing electrical muscle property change, and placement location drift.

All of these problems point toward a long term heart failure protocol and experiment for an answer. The method would then need to be reduced to practice, developing and incorporating low-power low-noise electronics into existing implanted devices. The heart failure detection system would need a communication channel to the patient and/or the doctor.

6.2 CONCLUSION

There are three important questions regarding admittance measurement that this dissertation answers. The first question is: “Which method for determining volume using traditional bio-impedance measurements is closest to the truth?” The answer is detailed in Chapter 2, where the use of a time-varying parallel conductance (G_p) removal method and a nonlinear conductance to volume equation (Wei’s equation) is shown to have less error when compared with 2-D echocardiography in mice.

The second question is: “Will the measurement scale to larger animals, and if so, is a new electrode configuration of admittance measurement that will not enter the left ventricle possible?” The answer to this question is given in Chapter 3. Through modeling work, it is shown that the admittance measurement does scale to larger animals. With the addition of multiple unused electrodes, the field is pulled away from the surrounding myocardium and closer to the catheter. This causes a change in the value of α used in the conductance to volume equation, and underlines the importance of careful calibration. A new electrode configuration of admittance is also modeled, and these models show that only a small portion of the signal will be due to surgical placement error.

The third question posed by this dissertation is its main focus. “Is it possible, using an electrode configuration that mimics pacemaker leads, to detect impending heart failure?” This question is explored in depth using three forms of volume modulation to determine that no secondary effects have caused conductance change. The three

methods to increase volume acutely in pigs were Neosynephrine injection, aortic banding, and LAD coronary artery occlusion. All three methods show an increase in volume causes an increase in measured blood conductance using the admittance technique, even when current methodology (RV pressure measurement, LV pressure measurement, and lung conductance measurement) fails to detect these volume increases.

Appendix 1: Full Protocols

The complete mouse and pig protocols for all studies are here, for reference for future graduate students interested in completing studies of their own which are similar. Many of the mistakes made over the course of the author's career could have been avoided with knowledge like this.

7.1 OPEN CHEST ACUTE PREPARATION IN PIGS

The open chest surgical preparation for a pig is a complicated mix of anti-arrhythmic agents (for hemodynamic stability) and positive inotropes (for increased blood pressure). It is often quite difficult to find the right proportion of stability and signal degradation which will give acceptable results and keep the subject alive for the duration of the experiment. In this experiment, the following protocol was used:

1. Pig is given Tealazol (0.5 ml) via intramuscular injection and transferred to the operating suite.
2. Isoflurane is given to induce an appropriate plane of anesthesia.
3. After the right carotid artery is cannulated and a pressure sensor is introduced for Aortic Pressure to monitor the pig's condition, a 150mg bolus of Amiodarone (an anti-arrhythmic) is given to prevent fibrillation upon opening the chest.
4. The chest is opened via sternotomy, and we let 30 minutes pass total to ensure that the pig has time to recover before the next Amiodarone bolus.
5. A second 150 mg bolus of Amiodarone is given. At this point, the hemodynamic system is severely depressed because Amiodarone is also a negative inotrope.

6. If the blood pressure ever dips below about 70 mmHg systolic, a 1mg bolus of Atropine is given to raise pressures. Normal systolic blood pressure in mammalian hearts is usually above 100 mmHg, but under anesthesia, we can expect a much lower number.
7. After the last bolus of Amiodarone is given, the pig is put on IV Lidocaine drip 1 mg/min for the remainder of the experiment. The Lidocaine acts as an analgesic without depressing the hemodynamic system.
8. Additionally, Lidocaine is used as a topical analgesic to prevent pain response when sewing an electrode patch or sonomicrometry crystal directly to the myocardium.
9. At this point, the rest of the instrumentation is added to the preparation. If, during the experiment, the additional Atropine and Lidocaine is not enough to increase pressures to a point which ensures survivability within about 5-10 minutes of the dose, Neosynephrine is given at 10-25 $\mu\text{g}/\text{min}$ (a positive inotrope).

7.2 CLOSED CHEST ACUTE CONTRACTILITY STUDIES IN MICE

1. Anesthetize mouse using Isoflurane container and maintain anesthesia using isoflurane delivered via respirator.
2. Record body weight, length, and sex in lab notebook and in Chart in Window > Notebook.
3. Insert IV for dobutamine
4. The chest will be opened via an anterior thoracotomy.
5. Insert catheter into LV via apical stick.

6. Record baseline admittance magnitude (conductance) and phase at 20 kHz, and pressure data, and analyze loops to ensure correct catheter placement.
7. Start Dobutamine drip
8. Wrap the IVC with umbilical tape for occlusions.
9. TIME = 00:00:00
10. TIME = 00:06:00
11. Unplug the Admittance Catheter from the RamsES box and replace with mouse surface probe.
12. Record admittance magnitude and phase using the mouse surface probe (for myocardial properties measurement). Mark the digital record with information about the data.
13. Re-seat the surface probe
14. Repeat steps 12-13 a total of N=2 times. (Last 2 steps
15. Unplug the mouse surface probe from the RamsES box and replace with the Scisense admittance catheter.
16. Occlude the IVC for 3 seconds (or long enough to ensure ESPVR is calculable).
17. Record pressure, admittance magnitude, and admittance phase data at 20 kHz during the occlusions and mark the record for future analysis.
18. Repeat steps 16-17 for N = 3 times total. (Last 2 steps)
19. TIME = 00:12:00
20. Increase the dobutamine drip
21. Repeat steps 9-20 for a total of N = 4 times (3 more times).
22. Attach flow probe.
23. Measure aortic flow using EM flow probe.

24. Extract blood from LV, measure conductivity using surface probe in 37°C water bath.
25. Euthanize animal and measure heart weight and LV weight.

7.3 OPEN CHEST 1 WK AORTIC BAND HEART FAILURE MICE

1. Anesthetize mouse using Isoflurane container and maintain anesthesia using isoflurane delivered via respirator.
2. Record body weight, length, and sex in lab notebook and in Chart in Window > Notebook.
3. The chest will be opened via an anterior thoracotomy.
4. Insert catheter into LV via apical stick.
5. Record baseline admittance magnitude (conductance) and phase at 20 kHz, and pressure data, and analyze loops to ensure correct catheter placement.
6. Wrap the IVC with umbilical tape and occlude for 3 seconds (or long enough to ensure ESPVR is calculable).
7. Record pressure, admittance magnitude, and admittance phase data at 20 kHz during the occlusion and mark the record for future analysis.
8. Repeat steps 7-8 for N = 3 times total.
9. Analyze Pressure-Conductance loops to ensure that a good data set has been taken, otherwise, reposition catheter and repeat steps 7-9.
10. Record admittance magnitude and phase using the mouse surface probe (for myocardial properties measurement). Mark the digital record with information about the data.
11. Re-seat the surface probe
12. Repeat steps 10-11 a total of N=2 times.

13. Attach flow probe.
14. Measure aortic flow using EM flow probe.
15. Extract blood from LV, measure conductivity using surface probe in 37oC water bath.
16. Euthanize animal and measure heart weight and LV weight.

References

- [1] P. A. McCullough, E. F. Philbin, J. A. Spertus, S. Kaatz, K. R. Sandberg, and W. D. Weaver, "Confirmation of a heart failure epidemic: findings from the Resource Utilization Among Congestive Heart Failure (REACH) study," *J Am Coll Cardiol*, vol. 39, pp. 60-9, Jan 2 2002.
- [2] D. Lloyd-Jones, R. Adams, M. Carnethon, G. De Simone, T. B. Ferguson, K. Flegal, E. Ford, K. Furie, A. Go, K. Greenlund, N. Haase, S. Hailpern, M. Ho, V. Howard, B. Kissela, S. Kittner, D. Lackland, L. Lisabeth, A. Marelli, M. McDermott, J. Meigs, D. Mozaffarian, G. Nichol, C. O'Donnell, V. Roger, W. Rosamond, R. Sacco, P. Sorlie, R. Stafford, J. Steinberger, T. Thom, S. Wasserthiel-Smoller, N. Wong, J. Wylie-Rosett, and Y. Hong, "Heart disease and stroke statistics--2009 update: a report from the American Heart Association Statistics Committee and Stroke Statistics Subcommittee," *Circulation*, vol. 119, pp. 480-6, Jan 27 2009.
- [3] J. Baan, T. T. Jong, P. L. Kerkhof, R. J. Moene, A. D. van Dijk, E. T. van der Velde, and J. Koops, "Continuous stroke volume and cardiac output from intraventricular dimensions obtained with impedance catheter," *Cardiovasc Res*, vol. 15, pp. 328-34, Jun 1981.
- [4] J. Baan, E. T. Vandervelde, H. G. Debruin, G. J. Smeenk, J. Koops, A. D. Vandijk, D. Temmerman, J. Senden, and B. Buis, "Continuous Measurement of Left-Ventricular Volume in Animals and Humans by Conductance Catheter," *Circulation*, vol. 70, pp. 812-823, 1984.
- [5] M. D. Feldman, J. M. Erikson, Y. Mao, C. E. Korcarz, R. M. Lang, and G. L. Freeman, "Validation of a mouse conductance system to determine LV volume: comparison to echocardiography and crystals," *Am J Physiol Heart Circ Physiol*, vol. 279, pp. H1698-707, Oct 2000.
- [6] A. T. Kottam, J. Porterfield, K. Raghavan, D. Fernandez, M. D. Feldman, J. W. Valvano, and J. A. Pearce, "Real time pressure-volume loops in mice using complex admittance: measurement and implications," *Conf Proc IEEE Eng Med Biol Soc*, vol. 1, pp. 4336-9, 2006.
- [7] K. Raghavan, A. T. Kottam, J. W. Valvano, and J. A. Pearce, "Design of a wireless telemetric backpack device for real-time in vivo measurement of pressure-volume loops in conscious ambulatory rats," *Conf Proc IEEE Eng Med Biol Soc*, vol. 2008, pp. 993-6, 2008.
- [8] K. Raghavan, J. E. Porterfield, A. T. G. Kottam, M. D. Feldman, D. Escobedo, J. W. Valvano, and J. A. Pearce, "Electrical Conductivity and Permittivity of Murine Myocardium," *Ieee Transactions on Biomedical Engineering*, vol. 56, pp. 2044-2053, Aug 2009.

- [9] K. Raghavan, C. L. Wei, A. Kottam, D. G. Altman, D. J. Fernandez, M. Reyes, J. W. Valvano, M. D. Feldman, and J. A. Pearce, "Design of instrumentation and data-acquisition system for complex admittance measurement," *Biomed Sci Instrum*, vol. 40, pp. 453-7, 2004.
- [10] M. Reyes, M. E. Steinhilper, J. A. Alvarez, D. Escobedo, J. Pearce, J. W. Valvano, B. H. Pollock, C. L. Wei, A. Kottam, D. Altman, S. Bailey, S. Thomsen, S. Lee, J. T. Colston, J. H. Oh, G. L. Freeman, and M. D. Feldman, "Impact of physiological variables and genetic background on myocardial frequency-resistivity relations in the intact beating murine heart," *Am J Physiol Heart Circ Physiol*, vol. 291, pp. H1659-69, Oct 2006.
- [11] C. L. Wei, J. W. Valvano, M. D. Feldman, D. Altman, A. Kottam, K. Raghavan, D. J. Fernandez, M. Reyes, D. Escobedo, and J. A. Pearce, "Evidence of time-varying myocardial contribution by in vivo magnitude and phase measurement in mice," *Conf Proc IEEE Eng Med Biol Soc*, vol. 5, pp. 3674-7, 2004.
- [12] J. Baan, T. T. A. Jong, P. L. M. Kerkhof, R. J. Moene, A. D. Vandijk, E. T. Vandervelde, and J. Koops, "Continuous Stroke Volume and Cardiac-Output from Intraventricular Dimensions Obtained with Impedance Catheter," *Cardiovascular Research*, vol. 15, pp. 328-334, 1981.
- [13] C. L. Wei, J. W. Valvano, M. D. Feldman, M. Nahrendorf, R. Peshock, and J. A. Pearce, "Volume catheter parallel conductance varies between end-systole and end-diastole," *Ieee Transactions on Biomedical Engineering*, vol. 54, pp. 1480-1489, Aug 2007.
- [14] P. Pacher, T. Nagayama, P. Mukhopadhyay, S. Batkai, and D. A. Kass, "Measurement of cardiac function using pressure-volume conductance catheter technique in mice and rats," *Nat Protoc*, vol. 3, pp. 1422-34, 2008.
- [15] J. Baan and E. T. Van der Velde, "Sensitivity of left ventricular end-systolic pressure-volume relation to type of loading intervention in dogs," *Circ Res*, vol. 62, pp. 1247-58, Jun 1988.
- [16] C. L. Wei, J. W. Valvano, M. D. Feldman, and J. A. Pearce, "Nonlinear conductance-volume relationship for murine conductance catheter measurement system," *Ieee Transactions on Biomedical Engineering*, vol. 52, pp. 1654-1661, Oct 2005.
- [17] J. E. Porterfield, A. T. Kottam, K. Raghavan, D. Escobedo, J. T. Jenkins, E. R. Larson, R. J. Trevino, J. W. Valvano, J. A. Pearce, and M. D. Feldman, "Dynamic Correction for Parallel Conductance, GP, and Gain Factor, $\{\alpha\}$, in Invasive Murine Left Ventricular Volume Measurements," *J Appl Physiol*, Aug 20 2009.

- [18] E. Braunwald, "Braunwald's Heart Disease. A Textbook of Cardiovascular Medicine ", 7th ed: Saunders (Elsevier), 2005, p. 540.
- [19] E. Braunwald, "Braunwald's Heart Disease. A Textbook of Cardiovascular Medicine ", 7th ed: Saunders (Elsevier), 2005, p. 499.
- [20] E. Braunwald, "Braunwald's Heart Disease. A Textbook of Cardiovascular Medicine ", 7th ed: Saunders (Elsevier), 2005, p. 515.
- [21] J. G. Cleland, J. C. Daubert, E. Erdmann, N. Freemantle, D. Gras, L. Kappenberger, and L. Tavazzi, "The effect of cardiac resynchronization on morbidity and mortality in heart failure," *N Engl J Med*, vol. 352, pp. 1539-49, Apr 14 2005.
- [22] P. B. Adamson, A. Magalski, F. Braunschweig, M. Bohm, D. Reynolds, D. Steinhaus, A. Luby, C. Linde, L. Ryden, B. Cremers, T. Takle, and T. Bennett, "Ongoing right ventricular hemodynamics in heart failure: clinical value of measurements derived from an implantable monitoring system," *J Am Coll Cardiol*, vol. 41, pp. 565-71, Feb 19 2003.
- [23] D. Lloyd-Jones, R. Adams, M. Carnethon, G. De Simone, T. B. Ferguson, K. Flegal, E. Ford, K. Furie, A. Go, K. Greenlund, N. Haase, S. Hailpern, M. Ho, V. Howard, B. Kissela, S. Kittner, D. Lackland, L. Lisabeth, A. Marelli, M. McDermott, J. Meigs, D. Mozaffarian, G. Nichol, C. O'Donnell, V. Roger, W. Rosamond, R. Sacco, P. Sorlie, R. Stafford, J. Steinberger, T. Thom, S. Wasserthiel-Smoller, N. Wong, J. Wylie-Rosett, and Y. Hong, "Heart disease and stroke statistics--2009 update: a report from the American Heart Association Statistics Committee and Stroke Statistics Subcommittee," *Circulation*, vol. 119, pp. e21-181, Jan 27 2009.
- [24] A. Magalski, P. Adamson, F. Gadler, M. Boehm, D. Steinhaus, D. Reynolds, K. Vlach, C. Linde, B. Cremers, B. Sparks, and T. Bennett, "Continuous ambulatory right heart pressure measurements with an implantable hemodynamic monitor: a multicenter, 12-month follow-up study of patients with chronic heart failure," *J Card Fail*, vol. 8, pp. 63-70, Apr 2002.
- [25] L. Luthje, T. Drescher, D. Zenker, and D. Vollmann, "Detection of heart failure decompensation using intrathoracic impedance monitoring by a triple-chamber implantable defibrillator," *Heart Rhythm*, vol. 2, pp. 997-9, Sep 2005.
- [26] D. Vollmann, H. Nagele, P. Schauerte, U. Wiegand, C. Butter, G. Zanolto, A. Quesada, A. Guthmann, M. R. Hill, and B. Lamp, "Clinical utility of intrathoracic impedance monitoring to alert patients with an implanted device of deteriorating chronic heart failure," *Eur Heart J*, vol. 28, pp. 1835-40, Aug 2007.
- [27] L. Wang, S. Lahtinen, L. Lentz, N. Rakow, C. Kaszas, L. Ruetz, L. Stylos, and W. H. Olson, "Feasibility of using an implantable system to measure thoracic

- congestion in an ambulatory chronic heart failure canine model," *Pacing Clin Electrophysiol*, vol. 28, pp. 404-11, May 2005.
- [28] C. M. Yu, L. Wang, E. Chau, R. H. Chan, S. L. Kong, M. O. Tang, J. Christensen, R. W. Stadler, and C. P. Lau, "Intrathoracic impedance monitoring in patients with heart failure: correlation with fluid status and feasibility of early warning preceding hospitalization," *Circulation*, vol. 112, pp. 841-8, Aug 9 2005.
- [29] A. T. G. Kottam, "Measurement of Electrical Admittance to Study the Onset and Progression of Myocardial Ischemia," in *Biomedical Engineering*. vol. Ph.D. Austin: The University of Texas, 2006, p. 103.
- [30] A. Kottam and J. A. Pearce, "Electric field penetration depth of myocardial surface catheters and the measurement of myocardial resistivity," *Biomed Sci Instrum*, vol. 40, pp. 155-60, 2004.
- [31] J. W. Gaynor, M. P. Feneley, S. A. Gall, Jr., G. W. Maier, J. A. Kisslo, J. W. Davis, J. S. Rankin, and D. D. Glower, Jr., "Measurement of left ventricular volume in normal and volume-overloaded canine hearts," *Am J Physiol*, vol. 266, pp. H329-40, Jan 1994.
- [32] J. G. Lainchbury, D. M. Meyer, M. Jougasaki, J. C. Burnett, Jr., and M. M. Redfield, "Effects of adrenomedullin on load and myocardial performance in normal and heart-failure dogs," *Am J Physiol Heart Circ Physiol*, vol. 279, pp. H1000-6, Sep 2000.
- [33] K. Raghavan, J. E. Porterfield, A. T. Kottam, M. D. Feldman, D. Escobedo, J. W. Valvano, and J. A. Pearce, "Electrical conductivity and permittivity of murine myocardium," *IEEE Trans Biomed Eng*, vol. 56, pp. 2044-53, Aug 2009.
- [34] C. Jacoby, A. Molojavyi, U. Flogel, M. W. Merx, Z. Ding, and J. Schrader, "Direct comparison of magnetic resonance imaging and conductance microcatheter in the evaluation of left ventricular function in mice," *Basic Res Cardiol*, vol. 101, pp. 87-95, Jan 2006.
- [35] J. M. Nielsen, S. B. Kristiansen, S. Ringgaard, T. T. Nielsen, A. Flyvbjerg, A. N. Redington, and H. E. Botker, "Left ventricular volume measurement in mice by conductance catheter: evaluation and optimization of calibration," *Am J Physiol Heart Circ Physiol*, vol. 293, pp. H534-40, Jul 2007.
- [36] E. B. Lankford, D. A. Kass, W. L. Maughan, and A. A. Shoukas, "Does volume catheter parallel conductance vary during a cardiac cycle?," *Am J Physiol*, vol. 258, pp. H1933-42, Jun 1990.

- [37] D. Georgakopoulos and D. A. Kass, "Estimation of parallel conductance by dual-frequency conductance catheter in mice," *Am J Physiol Heart Circ Physiol*, vol. 279, pp. H443-50, Jul 2000.
- [38] D. Georgakopoulos, W. A. Mitzner, C. H. Chen, B. J. Byrne, H. D. Millar, J. M. Hare, and D. A. Kass, "In vivo murine left ventricular pressure-volume relations by miniaturized conductance micromanometry," *Am J Physiol*, vol. 274, pp. H1416-22, Apr 1998.
- [39] P. Steendijk, G. Mur, E. T. Van Der Velde, and J. Baan, "The four-electrode resistivity technique in anisotropic media: theoretical analysis and application on myocardial tissue in vivo," *IEEE Trans Biomed Eng*, vol. 40, pp. 1138-48, Nov 1993.
- [40] WhitePa and A. N. Redington, "Right ventricular volume measurement: can conductance do it better?," *Physiol Meas*, vol. 21, pp. R23-41, Aug 2000.
- [41] K. Uemura, T. Kawada, M. Sugimachi, C. Zheng, K. Kashihara, T. Sato, and K. Sunagawa, "A self-calibrating telemetry system for measurement of ventricular pressure-volume relations in conscious, freely moving rats," *Am J Physiol Heart Circ Physiol*, vol. 287, pp. H2906-13, Dec 2004.
- [42] Millar, "Published papers: Pressure - mouse / rat," in http://www.millarinstruments.com/papers/papers_pres_m_r.php. vol. 2008, M. Instruments, Ed. Houston, TX, 2008.
- [43] S. Kun and R. A. Peura, "Analysis of conductance volumetric measurement error sources," *Med Biol Eng Comput*, vol. 32, pp. 94-100, Jan 1994.
- [44] B. Hille, *Ion channels of excitable membranes*, 3rd ed. Sunderland, Mass.: Sinauer, 2001.
- [45] C. L. Wei and M. H. Shih, "Calibration Capacity of the Conductance-to-Volume Conversion Equations for the Mouse Conductance Catheter Measurement System," *Ieee Transactions on Biomedical Engineering*, vol. 56, pp. 1627-1634, Jun 2009.
- [46] T. J. Faes, H. A. van der Meij, J. C. de Munck, and R. M. Heethaar, "The electric resistivity of human tissues (100 Hz-10 MHz): a meta-analysis of review studies," *Physiol Meas*, vol. 20, pp. R1-10, Nov 1999.
- [47] P. Steendijk, E. T. van der Velde, and J. Baan, "Dependence of anisotropic myocardial electrical resistivity on cardiac phase and excitation frequency," *Basic Res Cardiol*, vol. 89, pp. 411-26, Sep-Oct 1994.
- [48] M. R. Graham, R. K. Warrian, L. G. Girling, L. Doiron, G. R. Lefevre, M. Cheang, and W. A. Mutch, "Fractal or biologically variable delivery of cardioplegic solution

- prevents diastolic dysfunction after cardiopulmonary bypass," *J Thorac Cardiovasc Surg*, vol. 123, pp. 63-71, Jan 2002.
- [49] E. Glusa and F. Markwardt, "Characterisation of postjunctional alpha-adrenoceptors in isolated human femoral veins and arteries," *Naunyn Schmiedebergs Arch Pharmacol*, vol. 323, pp. 101-5, Jun 1983.
- [50] J. Pepke-Zaba, T. W. Higenbottam, A. T. Dinh-Xuan, C. Ridden, and T. Kealey, "Alpha-adrenoceptor stimulation of porcine pulmonary arteries," *Eur J Pharmacol*, vol. 235, pp. 169-75, Apr 28 1993.
- [51] R. C. Bourge, W. T. Abraham, P. B. Adamson, M. F. Aaron, J. M. Aranda, Jr., A. Magalski, M. R. Zile, A. L. Smith, F. W. Smart, M. A. O'Shaughnessy, M. L. Jessup, B. Sparks, D. L. Naftel, and L. W. Stevenson, "Randomized controlled trial of an implantable continuous hemodynamic monitor in patients with advanced heart failure: the COMPASS-HF study," *J Am Coll Cardiol*, vol. 51, pp. 1073-9, Mar 18 2008.

Vita

John Edward Porterfield is a native Texan and was born at Methodist Hospital in San Antonio, across the street from the laboratory at UT Health Science Center in San Antonio where the bulk of his experimental work was completed. In 2000 he entered Oklahoma State University in Stillwater, OK where he received his B.S. in Electrical and Computer Engineering in 2004. After this degree he continued his education at The University of Texas at Austin and in 2006 received his M.S. in Electrical Engineering (with Biomedical Instrumentation focus) under guidance from Dr. John Pearce, who also advised his Ph.D.

Permanent Address: 2916 W. Lexington Way, Edmond, OK 73003

This manuscript was typed by the author.